MECHANOSYNTHESIS AND CHARACTERIZATION OF $Bi_{1-x}Gd_xFeO_3$ MULTIFERROIC MATERIALS

A THESIS SUBMITTED IN PARTIAL FULFILMENT OF THE REQUIREMENTS FOR THE DEGREE OF MASTER OF TECHNOLOGY

IN

MATERIALS SCIENCE AND METALLURGICAL ENGINEERING

By

ALOK MISHRA

ROLL No. - 600802001

Under the Guidance of

Dr. Puneet Sharma

SCHOOL OF PHYSICS AND MATERIAL SCIENCE

THAPAR UNIVERSITY PATIALA

PUNJAB - 147004, INDIA

15 JULY 2009

Dedicated to

My

Parents

And

Teachers

CERTIFICATE

This is to certify that the thesis entitled "MECHANOSYNTHESIS AND CHARACTERIZATION OF $Bi_{1-x}Gd_xFeO_3$ MULTIFERROIC MATERIALS" submitted by **Mr. ALOK MISHRA** Roll No. 600802001 in partial fulfillment of the requirement for the award of the degree of **MASTER OF TECHNOLOGY** in Materials Science and Metallurgical Engineering, Thapar University Patiala, is a record of candidate's own work carried out by him under my supervision. The matter embodied in this report is of the candidate's own record and not submitted to any other university in any part or full form for the award of any degree.

(Alok Mishra)

The thesis work has been carried out from 05-01-2010 to 15-07- 2010.

Supervisor

(Dr. Puneet Sharma)

Assistant Professor

Thapar University, Patiala

Countersigned by

(Dr. O.P.Pandey)

Professor and Head of SPMS

Thapar University, Patiala

(Dr. R.K.Sharma) 29.7.10

Dean Academic Affairs

Thapar University, Patiala

ACKNOWLEDGEMENT

I would like to express my deepest gratitude to my supervisor Dr. Puneet Sharma for the inspiring guidance, support, encouragement and time commitment during this thesis work. I could not finish my study without his help and encouragement. I believe what I have learnt from him would greatly benefit my future career.

I wish to express my sincere thanks to Dr. O.P. Panday, Professor and Head, School of Physics and Materials Science for permitting and providing the necessary facilities for carrying out thesis.

I am highly grateful to Professor K. K. Raina, Dr. Kulvir Singh, DR. D.P. Singh and Dr. S.D. Tiwari School of Physics & Material Science, for their kind help and valuable suggestions and special attention throughout my work. It is due to their moral encouragement, love and providing me fountain of inspiration all sorts of assistance from time to time into up-bringing me upto this stage.

I am highly thankful to all Ph.D. Scholar's Mr. Ravi Shukla, Mr. Vishal Chaudhary, Mr. Akshay Kumar, Mr.Praveen Paliwal, Jasmeet Gill, Gurbinder Kaur of the department for providing all kind of support for carrying out the work.

I would like to give my sincere thanks to Mr. Purushotam Kumar Singh (Lab. Superintendent) for carrying out sample characterization and also thankful to Mr. jant singh for his kindly support.

I would also like to give many thanks to all my seniors and friends for their support.

I am deeply thankful to my family, their moral support and patience has borne fruit through completion of this thesis which will result in award of the prestigious degree of M.Tech. in Materials Science & Engineering.

Alok mishra

(ALOK MISHRA)

CONTENTS

CERTIFICATE i

ACKNOWLEDGEMENT ii-iii

ABSTRACT iv

LIST OF FIGURES v-vi

LIST OF TABLES vii

CHAPTER 1: INTRODUCTION **1-16**

1.1. Background of Multiferroics 1-3

1.2 .Multiferroics Materials 3-5

1.3. Structure of Multiferroics 5-6

1.4. Different Types of Multiferroics 6-7

1.4.1. Type-I Multiferroic 7

1.4.1.1. Perovskite Types Multiferroics 7-8

1.4.1.2. Ferroelectricity Due to Lone Pairs 8-9

1.4.1.3. Ferroelectricity Due to Charge Ordering 9

1.4.1.4. Geometrically Frustrated Multiferroics 9-10

1.4.1.5. Magnetically Driven Ferroelectricity 10-11

1.4.2. Type-II Multiferroics 11

1.4.2.1. Magnetic Multiferroics 11

1.4.2.2. Multiferroic with Collinear Magnetic Structure 11-12

1.5. Application of multiferroics 12-13

1.6. Synthesis of multiferroic materials 13

1.6.1. Auto Combustion Route 13-14

1.6.1.1 Procedure 14-15

1.6.2. Sol-gel Route 15

1.6.3. High energy Ball Milling Route 15-16

CHAPTER2: LITERATURE REVIEW 17-26

CHAPTER3: EXPERIMENTALPROCEDURE 27-29

CHAPTER4: RESULTS AND DISCUSSION 30-45

4.1. Thermal Analysis of the milled powder 30-31

4.2. X-ray diffraction of the synthesis samples 31-35

4.3. FTIR spectrum of $Bi_{1-x}Gd_xFeO_3$ (x=0.0, 0.05, 0.1, 0.15, and 0.2) 35-37

4.4. P-E Loop Measurements 37-39

4.5. Measurement of Dielectric Properties 39-41

4.6. SEM image of $Bi_{1-x}Gd_xFeO_3$ (x=0.0, 0.1, 0.2) 42-45

CHAPTER5: CONCLUSION AND FUTURE WORK 46-47

REFERENCES 48-51

ABSTRACT

In the Present work multiferroic materials $BiFeO_3$ were synthesized by high energy ball milling (HEBM) followed by thermal annealing at various temperatures. Further the effect of Gd substitution for Bi was investigated. The concentration of Gd was varied in the range of x=0.0 – 0.20). Phase characterization was carried out by X-ray diffraction. It is found that with increasing Gd content the impurity phase is decreased and single $BiFeO_3$ phase is found at Gd (x = 0.1). Further increase in Gd content from x = 0.1 to 0.2 the impurity phase increases. The room temperature dielectric properties of pure and substituted $BiFeO_3$ were measured in the frequency range from 20 Hz to 1MHz using LCR meter. For all studied samples dielectric constant increased from 110 (x=0.0) to 250 (x=0.10) and then decreases. The dielectric loss found to be more for pure $BiFeO_3$ as compared to $Bi_{1-x}Gd_xO_3$. The P-E loops are also shows that the maximum polarization is in $Bi_{0.9}Gd_{0.1}FeO_3$ as we increase the percent of Gd in Bi site the polarization becomes decrease. Scanning electron micrograph of $Bi_{1-x}GdxFeO_3$ (x=0.0, 0.1, 0.2) sintered sample shows that as we increase the concentration of Gd the grain size decrease. The grain shape is also changed with doping.

LIST OF FIGURES

Chapter 1 **Page Number**

Figure 1.1 (i): The relationship between multiferroic and magneto electric materials 5

Figure 1.2 (ii): Time-reversal and spatial-inversion symmetry in ferroics 5

Figure 1.3 (iii): The ABO_3 type perovskite structure 6

Chapter 3

Figure 3.1: Flow chart of the experimental work 29

Chapter 4

Figure 4.1: DTA/TGA curve of the milled (up to 10 hours) powder samples 31

Figure 4.2 (i): X-ray diffraction pattern of raw materials and after milled the raw materials up to 10 hours 32

Figure 4.2 (ii): X-ray diffraction pattern of $BiFeO_3$ after calcined at different temperature range 33

Figure 4.2 (iii): X-ray diffraction pattern of $Bi_{1-x}Gd_xFeO_3$ (x=0.05, 0.10, 0.15, 0.20) 34

Figure 4.2 (iv): Variation in the crystal size with the GD substitution 35

Figure 4.3 (i): FTIR spectrum of $BiFeO_3$ calcined at different temperature 36

Figure 4.3 (ii): FTIR spectrum of $Bi_{1-x}Gd_xFeO_3$ (x=0.05, 0.10, 0.15, 0.20) 37

Figure 4.4 (i): P-E loop in $Bi_{1-x}Gd_xFeO_3$ (x=0.05, 0.1, 0.15, and 0.2) 38

Figure 4.4 (ii): Polarization behavior of the sample with Gd substitution 39

Figure 4.5 (i): Dielectric constant in $Bi_{1-x}Gd_xFeO_3$ (x=0.05, 0.10, 0.15, 0.20) 40

Figure 4.5 (ii): Dielectric losses in $Bi_{1-x}Gd_xFeO_3$ (x=0.05, 0.10, 0.15, 0.20) 41

Figure 4.6 (i): SEM of sample $Bi_{1-x}Gd_xFeO_3$ at 1000X 43

Figure 4.6 (ii): SEM of sample $Bi_{1-x}Gd_xFeO_3$ at 2500X 44

Figure 4.6 (iii): SEM of sample $Bi_{1-x}Gd_xFeO_3$ at 5000X 45

LIST OF TABLES

Chapter 4 **Page Number**

Table 4.4(i): Polarization measurements of the Gd doped in the
$Bi_{1-x}Gd_xFeO_3$ (x=0.05, 0.10, 0.15, 0.20) samples 38

CHAPTER 1
INTRODUCTION

1.1. Background of Multiferroics

Electricity and magnetism were combined into one common discipline in the 19th century, culminating in the Maxwell equations. But electric and magnetic ordering in solids is most often considered separately and usually with good reason: the electric charges of electrons and ions are responsible for the charge effects, whereas electron spins govern magnetic properties. There are, however, cases where these degrees of freedom couple strongly. For example, in the new, large field of spintronics, the effects of spins on the transport properties of solids (and vice versa) allow the possibility to control one by the other. The finding of a strong coupling of magnetic and electric degrees of freedom in insulators can be traced back to Pierre Curie, but the real beginning of this field started in 1959 with a short remark by Landau and Lifshitz in a volume of their Course of Theoretical Physics [1]. "Let us point out two more phenomena, which, in principle, could exist. One is piezomagnetism, which consists of linear coupling between a magnetic field in a solid and a deformation (analogous to piezoelectricity). The other is a linear coupling between magnetic and electric fields in a media, which would cause, for example, a magnetization proportional to an electric field. Both these phenomena could exist for certain classes of magneto crystalline symmetry [2]. A new twist in this problem was the idea that not only can strong cross-coupling of responses exist in solids (i.e., the appearance of magnetization **M** in an electric field **E**, or the inverse effect of electric polarization **P** generated by the application of magnetic field **H**), but that there may exist systems in which two types of ordering ferromagnetism, the spontaneous ordering of orbital and spin magnetic moments, and ferroelectricity, the spontaneous ordering of electric dipole moments can coexist in one material in the absence of external electric and magnetic fields. Schmid called these materials as a multiferroics material [3]. Boracites

were probably the first known multiferroics [4], and soon several others were either found in nature, or synthesized artificially [5]. In 2003, Ramesh's group successfully grew thin films of one of the most popular multiferroics, $BiFeO_3$ [6]. The multiferroic properties of bulk $BiFeO_3$ are fairly weak, but in thin-film form they are greatly enhanced. The second major experimental development, also in 2003, was the discovery of a novel class of multiferroics, in which magnetism and ferroelectricity do not just coexist, but in which magnetism causes ferroelectricity. Tokura and Kimura discovered this phenomenon in $TbMnO_3$ [7] and Cheong found a similar effect in $TbMn_2O_5$ [8].

Electricity and magnetism are properties which are closely linked to each other. This link is dynamic in essence, as moving charges generate a magnetic field and a changing magnetic field produces an electric field. This forms the basis of Maxwell's equations. In a solid, similar coupling were first considered by Pierre Curie [9] between the magnetization M and electric polarization P. This magneto-electric (ME) effect was recently understood to e potentially important for applications in information technology; it would allow magnetic information to be written electrically (with low energy consumption) and to be read magnetically. The ME effect was demonstrated and studied in the 1960s in Russia [10], and since then, many so called 'multiferroic' materials have been identified [11]. However, so far the magnitude and operating temperatures of any observed ME coupling have been too small for applications. In fact, the only known multiferroic material of potential practical interest is bismuth ferrite, $BiFeO_3$ which is actually antiferromagnetism below T_N=370C and ferroelectric with a high Curie temperature: T_c = 820C [12].

The term multiferroic was first used by H. Schmid in 1994. His definition referred to multiferroics as single phase materials which simultaneously possess two or more primary ferroic properties. Today the term multiferroic has been expanded to include materials which exhibit any type of long range magnetic ordering, spontaneous electric polarization, and/or ferroelectricity. Working under this expanded definition the history of magneto electric multiferroics can be traced back to the 1960s [13]. In the most

general sense the field of multiferroics was born from studies of magneto electric systems [14]. In 2003 the discovery of large ferroelectric polarization in epitaxially grown thin films of $BiFeO_3$ [15] and the discovery of strong magnetic and electric coupling in orthorhombic $TbMnO_3$ [16] and $TbMn_2O_5$ [17] re-stimulated activity in the field of multiferroics. To understand the basic phenomena in the field of multiferroics, and appreciate the main achievements and remaining problems in this field, it is necessary to classify multiferroics by the microscopic mechanism that determines their properties.

1.2. Multiferroics Materials

Multiferroics are materials which display both ferroelectric and magnetic ordering and are promising for innovative devices such as transducers, sensors [18] and memories for data storage. Single-phase materials in which ferromagnetism and ferroelectricity arise independently also exist but are rare [19]. A rare class of materials, known as multiferroics, holds great promise for future applications, for example as data storage devices or sensors. However, progress has been hampered by the low operation temperatures and high magnetic fields required to control a property of the materials known as electric polarization. In a ferromagnetic material, the individual magnetic moments of its atoms are aligned in one direction. In a ferroelectric material, if the positive and negative electric charges are uniformly separated electric polarization is generated. In multiferroic materials, magnetism and ferroelectricity occur simultaneously and both properties are coupled to each other. Multiferroic materials can be considered as being materials presenting at least two ferroic states. These ferroic states are ferroelectricity, ferroelectricity and ferromagnetism. Thus, as a logical dentition to the term multiferroic, we could use the term multiferroic to any material presenting two of these three properties. However, the most interesting combination was thought to be materials presenting ferroelectricity and ferromagnetism. Hill discussed the conditions required for ferroelectricity and ferromagnetism to be compatible in transition metal oxides, and declared them to be rarely met [19]. Thus, the current trend is that any

material presenting simultaneously a polar state and a long range magnetic order is considered as a multiferroic.

Multiferroics have been formally defined as materials that exhibit more than one primary ferroic order parameter simultaneously (i.e. in a single phase) [20]. The four basic primary ferroic order parameters are ferromagnetism, ferroelectricity, ferroelectricity and ferrotoroidicity, the latter still being under debate. However, many researchers in the field consider materials as multiferroics only if they exhibit coupling between the order parameters. On the other hand, the definition of multiferroics can be expanded as to include non-primary order parameters, such as antiferromagnetism or ferrimagnetisms.

Typical multiferroics belong to the group of the perovskite transition metal oxides, and include rare-earth manganites and ferrites (e.g. $TbMnO_3$, $HoMn_2O_5$, and $LuFe_2O_4$). Other examples are the bismuth alloys $BiFeO_3$ and $BiMnO_3$, and non-oxides such as $BaNiF_4$.

Hexaferrites, compounds based on iron oxide, comprise a particularly interesting class of multiferroic materials and hold promise as novel high-temperature multiferroics. “Hexaferrites at present may be the best candidates for room-temperature multiferroics, as at least their magnetism exists up to room-temperature,” [21].

In the Hexaferrites $BaMg_{22}Fe_{12}O_{22}$ this compound is part of a class of multiferroics in which the ferroelectric polarization is generated by its unusual magnetic structure. The electric polarization is induced by so-called spin spirals, or cyclic variations in the orientation of the different magnetic moments along the crystal [22].

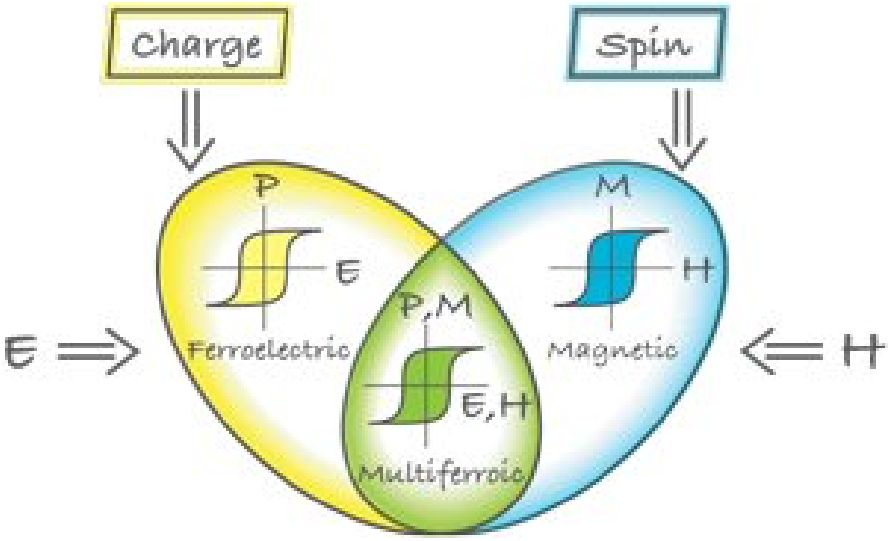

Figure1.2 (i). The relationship between multiferroic and magneto electric materials [23]

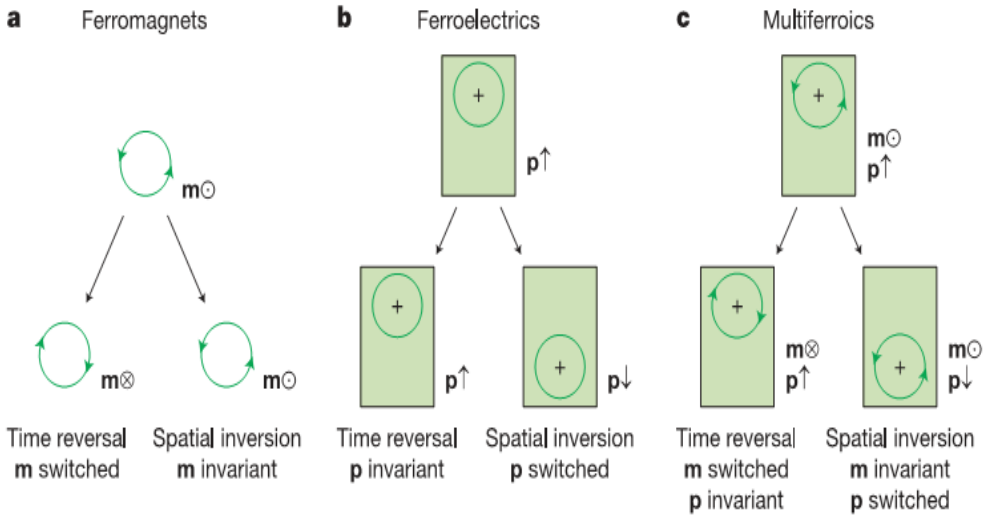

Figure1.2 (ii). Time-reversal and spatial-inversion symmetry in ferroics [23]

1.3. Structure of multiferroics

Multiferroics materials exhibits perovskite structure as shown in figure .the general formula of multiferroics materials is ABO_3, where A, B are cations and O

(anions) is oxygen which are situated at octahedron site of the lattice. A occupy the corner of the lattice and B occupy the centre.

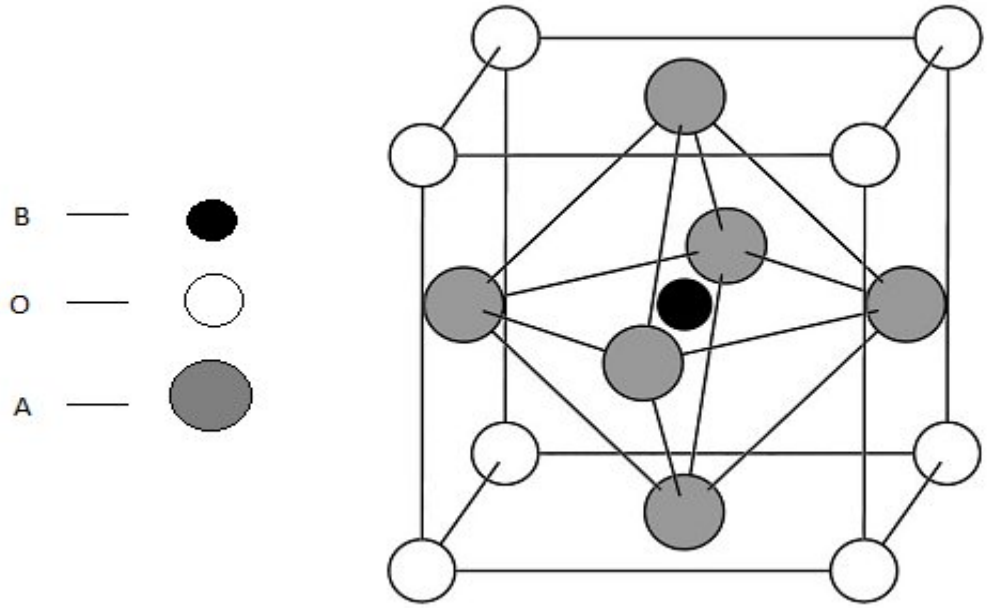

Figure1.3. The perovskite structure the small B cation (black) is at the centre of an octahedron of oxygen anions (gray). The large A cations (white) occupy the unit cell corners.

1.4. Types of Multiferroics

The microscopic origin of magnetism is basically the same in all magnets: it is the presence of localized electrons, mostly in the partially filled d or f shells of transition-metal or rare-earth ions, which have a corresponding localized spin, or magnetic moment. Exchange interactions between the localized moments lead to magnetic order. The situation with ferroelectrics is quite different. There are several different microscopic sources of ferroelectricity, and accordingly one can have different types of multiferroics. Generally, there are two groups of multiferroics. The first group, which can be called type-I multiferroics, contains those materials in which ferroelectricity and magnetism have different sources and appear largely independently of one another, though there is

some coupling between them. In these materials, ferroelectricity typically appears at higher temperatures than magnetism, and the spontaneous polarization **P** is often rather large (of order 10-100μC/cm^2). Examples are $BiFeO_3$ and $YMnO_3$. The second group, which we can call type-II multiferroics, is the relatively recently discovered materials [24] in which magnetism causes ferroelectricity, implying a strong coupling between the two. However, the polarization in these materials is usually much smaller (~10^{-2}μC/cm^2). Many groups are also investigating composite multiferroics that consist of known magnets and ferroelectrics in the form of multilayer and self-organized nanostructures [25].

1.4.1. Type-I multiferroics

Type-I multiferroics are "older" and more numerous. These are often good ferroelectrics, and the critical temperatures of the magnetic and ferroelectric transitions can be well above room temperature. Unfortunately, the coupling between magnetism and ferroelectricity in these materials is usually rather weak. The materials challenge for this group of multiferroics is to keep all their positive features, but enhance this coupling. As we will see later, the opposite problem exists for type-II multiferroics.

One can single out several different subclasses of type-I multiferroics, depending on the mechanism of ferroelectricity in them. We will focus on four of the major subclasses, but there are certainly others.

1.4.1.1. Perovskite types Multiferroic

Probably the best-known ferroelectrics are the perovskite like $BaTiO_3$ or $Pb(ZrTi)O_3$ (PZT). Magnetic and other properties of oxides and related compounds, and also many ferroelectrics [26] demonstrates that there seems to be mutual exclusion of magnetism and ferroelectricity in perovskite: Whereas for magnetism one needs partially filled d shells of a transition metal, practically all ferroelectric perovskite contain transition metal ions with an empty d shell, such as Ti^{4+}, Ta^{5+}, W^{6+}. Ferroelectricity in

these systems is caused by the off-centre shifts of the transition metal ion, which forms strong covalent bonds with one (or three) oxygen's, using their empty d states. And somehow, the presence of real d electrons in d^n configurations of magnetic transition metals suppresses this process, preventing ferroelectricity in magnetic perovskite. This so called" d^0 vs. d^n problem" was one of the first to be studied theoretically at the beginning of the recent revival of multiferroics [27].

1.4.1.2. Ferroelectricity Due to Lone Pairs

In $BiFeO_3$, and probably in $BiMnO_3$ and $PbVO_3$, Bi^{3+} and Pb^{2+} play the major role in the origin of ferroelectricity. In these ions, there are two outer 6s electrons that do not participate in chemical bonds. They are called lone pairs. They have a high polarizability the condition required for ferroelectricity in the classical description. More microscopically one can explain the origin of ferroelectricity in these compounds by ordering of these lone pairs in one direction. Apparently this is what happens in many Bi- and Pb-containing ferroelectrics and multiferroics such as $BiFeO_3$, but it also helps to improve the ferroelectric properties of Pb $(Zr_xTi_{1-x})O_3$. In usual perovskite-based ferroelectrics like $BaTiO_3$, the ferroelectric distortion occurs due to the displacement of B-site cation (Ti) with respect to the oxygen octahedral cage. Here the transition metal ion (Ti in $BaTiO_3$) requires an empty "d" shell since the ferroelectric displacement occurs due to the hopping of electrons between Ti "d" and O p atoms. This normally excludes any net magnetic moment because magnetism requires partially filled "d" shells. However, partially filled "d" shell on the B-site reduces the tendency of perovskite to display ferroelectricity.

In order for the coexistence of magnetism and ferroelectricity (multiferroic), one possible mechanism is lone-pair driven[28] where the A-site drives the displacement and partially filled "d" shell on the B-site contributes to the magnetism. Examples include $BiFeO_3$, $BiMnO_3$, and $PbVO_3$ [29]. In the above materials, the A-site cation (Bi^{3+}, Pb^{2+}) has a stereochemically active $6s^2$ lone-pair which causes the 6p (empty) orbital of Bi to

come closer in energy to the 2p orbitals of oxygen. This leads to hybridization between the 6p and 2p orbitals and drives the off-centring of the cation towards the neighbouring anion resulting in ferroelectricity.

1.4.1.3. Ferroelectricity Due to Charge Ordering

One more mechanism that can lead to ferroelectricity and to type-I multiferroicity can be charge ordering, often observed in transition metal compounds, especially those formally containing transition metal ions with different valence. If, after charge ordering, both sites and bonds turn out to be in equivalent, this can lead to ferroelectricity [30]. Such an order can occur in a compound containing ions of mixed valence and with geometrical or magnetic frustration. These ions form a polar arrangement, causing improper ferroelectricity (i.e. no ionic displacement). If magnetic ions are present, a coexisting magnetic order can be established and may be coupled to ferroelectricity.

Examples: One prominent example for a charge ordered multiferroic is $LuFe_2O_4$, which shows improper ferroelectricity below 330K [31]. The arrangements of the electrons arise from the charge frustration on a triangular lattice with the mixed valence state of Fe^{2+} and Fe^{3+} ions. Ferromagnetic behaviour occurs below 240 K.

1.4.1.4. Geometrically Frustrated Multiferroics

Geometric frustrated multiferroicity is related to a structural phase transition at high temperature. Several compounds belong to this important class of multiferroics: K_2SeO_4, Cs_2CdI_4, and hexagonal $RMnO_3$. These systems are proto-typical multiferroics which can be understood by competition between local interactions on several ion sites. For example, in hexagonal manganites h-$RMnO_3$ (R=Ho-Lu, Y), the ferroelectric polarization at high temperature is correlated to lattice distortions through off-centering of ions. Geometric frustration gives rise to novel spin arrangements at low temperature: The spins order in a variety of non-collinear, e.g. (in-plane) triangular to relieve the

geometric frustration. The coexistence of ferroelectric and magnetic order occurs together with a strong coupling between two disparate order parameters.

The mechanism of the ferroelectric ordering in hexagonal $RMnO_3$ is still questionable in scientific community and must be understood before a comprehensive picture of multiferroic phenomena in spin frustrated systems can be built. It is still matter of debate whether the geometric distortion is the origin of the electric polarization or whether the off-centring of Mn ions also contributes to the polarization.

Physical properties of geometric multiferroics are dominated by the behaviour of the d-shell electrons (e.g. orbitals) and of the rare earth elements with an unfilled f-shell. Hexagonal manganites show the largest deviation from perovskite structure due to the small size of rare-earth ion. Although geometrically frustrated multiferroics exhibit a simple chemistry, they provide a unique set of physical properties, such as rich phase diagrams or multiple frustrations. The strong coupling between ferroelectric and magnetic orders is represented by an anomaly in the static dielectric constant at magnetic phase transitions. Geometric frustrated ferroelectrics are prime candidates for device memory applications.

1.4.1.5. Magnetically Driven Ferroelectricity

Magnetically driven multiferroics are insulating materials, mostly oxides, in which macroscopic electric polarization is induced by magnetic long-range order. A necessary but not sufficient condition for the appearance of spontaneous electric polarization is the absence of inversion symmetry. In these materials inversion symmetry is broken by magnetic ordering. Such a symmetry breaking often occurs in so-called frustrated magnets, where competing interactions between spins favour unconventional magnetic orders. The microscopic mechanisms of magnetically induced ferroelectricity involve the polarization of electronic orbitals and relative displacement of ions in response to magnetic ordering.

Many multiferroics show the cycloid spiral ordering, in which spins rotate around an axis perpendicular to the propagation vector of the spiral. The induced electric polarization is orthogonal to the propagation vector and lies in the spiral plane. An abrupt change of the spiral plane induced by magnetic field is results in the corresponding rotation of the polarization vector. In $DyMnO_3$ this transition is accompanied by the 600% increase of dielectric constant. The microscopic mechanism of magneto electric coupling in spiral multiferroics involves spin-orbit coupling.

1.4.2. Type-II Multiferroics

1.4.2.1. Magnetic Multiferroics

The biggest excitement nowadays is caused by the discovery of a novel class of multiferroics in which ferroelectricity exists only in a magnetically ordered state and is caused by a particular type of magnetism [16, 17]. For example, in $TbMnO_3$ magnetic ordering appears at T_{N1}=41K, and at a lower temperature, T_{N2}=28K, the magnetic structure changes. It is only in the low-temperature phase that a nonzero electric polarization appears. Similar behaviour occurs in $TbMn_2O_5$.

$TbMnO_3$ showed that a magnetic field can strongly influence the electric polarization: e.g., in $TbMnO_3$ the polarization rotates (or "flops") by 90^o when a critical magnetic field is applied along a certain direction [16]. In $TbMn_2O_5$ [17] the influence of an external field is even stronger: the polarization changes sign with field, and a field alternating between +1.5 and -1.5 Tesla leads to corresponding oscillations in the polarization. Since the discovery of these materials, a number of other type-II multiferroics with strong magneto electric coupling have been discovered and studied.

1.4.2.2. Multiferroic with collinear magnetic structures

The second group of magnetically driven ferroelectrics are those in which ferroelectricity appears in collinear magnetic structures that are all magnetic moments

aligned along a particular axis without the necessary involvement of the spin-orbit interaction. Polarization can appear in these materials as a consequence of exchange striction because the magnetic coupling varies with the atomic positions. The simplest example, found in Ca_3CoMnO_6 [32]. Ca_3CoMnO_6 consists of one-dimensional chains of alternating Co^{2+} and Mn^{4+} ions. At high temperature the distances between the ions along the chain are the same, the chain has inversion symmetry, and polarization is absent. Magnetic ordering, however, breaks inversion symmetry: the spins form a ↑↑↓↓ type magnetic structure. Due to an exchange striction the distortion of ferro and antiferro bonds (↑↑ and ↑↓) is different, the material becomes ferroelectric. [33]In the case of Ca_3CoMnO_6, exchange striction arises from transition metal ions with a different valence (Co^{2+} and Mn^{4+}). One can, however, get the same effect even for identical magnetic ions, when one takes into account that the exchange in transition metal oxides usually occurs via intermediate oxygen's and depends on both the distance between the metal ions and the metal-oxygen-metal bond angle. In $RMnO_3$ perovskite where R is a small rare earth, the Mn magnetic order in the basal plane is of the type ↑↑↓↓. As proposed by Sergienko, Sen, and Dagotto [34], exchange striction in this case can cause the oxygen ions to shift perpendicular to the Mn-Mn bonds, which produces a polarization along the direction of the shift.

1.5. Applications

Multiferroic materials have many applications in bulk form as well as in nano form in electronic devises. Now days the coating of multiferroics material is being used for better application. Multiferroic composite structures in bulk form are explored for high-sensitivity ac magnetic field sensors and electrically tunable microwave devices such as filters, oscillators and phase shifters (in which the ferri, ferro or antiferromagnetic resonance is tuned electrically instead of magnetically [35]. In multiferroic thin films, the coupled magnetic and ferroelectric order parameters can be exploited for developing magneto electronic devices. These include novel spintronics devices such as tunnel magneto resistance (TMR) sensors and spin valves with electric field tunable functions.

A typical TMR device consists of two layers of ferromagnetic materials separated by a thin tunnel barrier (~2 nm) made of a multiferroic thin film [37]. In such a device, spin transport across the barrier can be electrically tuned. In another configuration, a multiferroic layer can be used as the exchange bias pinning layer. If the antiferromagnetic spin orientations in the multiferroic pinning layer can be electrically tuned, then magneto resistance of the device can be controlled by the applied electric field [38]. One can also explore multiple state memory elements, where data are stored both in the electric and the magnetic polarizations.

1.6. Synthesis of Multiferroics Material by Different Route

Multiferroic material is synthesized by many methods. The multiferroics material has the good application in the area of sensor, and memory based devices. There are some methods to synthesize the multiferroic material like auto combustion method, sol-gel process, and high energy ball milling process are given below.

1.6.1. Auto combustion Route

One of the most widely used and useful method of preparation of ABO_3 is the combustion synthesis route using a fuel. The fuel used may be glycine, citric acid or urea. The precursor materials used for the synthesis of ABO_3 by auto combustion route are ANO_3 and BNO_3 solutions with a certain concentration level. Combustion synthesis is becoming one of the most popular methods for the preparation of a wide variety of materials, .The main advantage of using this technique is due to the simplicity, the broad applicability range, the self-purifying feature due to the high temperatures involved, the possibility of obtaining products in the desired size and shape. This method is rapidly emerging as one of the most-convenient methods for the preparation of oxide materials. An aqueous solution of a redox system constituted by the nitrate ions of the metal precursor, acting as oxidizer, and a fuel like urea, glycine, citric acid or many others is heated up to moderate temperatures and, upon dehydration, the strongly exothermic redox reaction develops, which is generally self-sustaining and provides the energy for

the formation of the oxide. Among the various wet chemical processes, the combustion route is found to be simple and cost effective for the synthesis of homogeneous, very fine, crystalline nanopowders without the intermediate decomposition and calcinations steps which other conventional synthesis routes would require. The process is based on the mixing of reactants that oxidize easily, such as metal nitrates, and an organic fuel, acting as a reducing agent. An external heat supply is needed to initiate the ignition of the mixture leading to a self-sustainment of an exothermic redox reaction. In this technique, based on the principles of the propellant chemistry, a thermally induced redox reaction takes place between an oxidant and a fuel. Many types of combustion synthesis exist which differ mainly in the physical state of the reactants or in the combustion modality. By combustion-based methods it is possible to produce monophasic nanopowders with homogeneous microstructure, at lower temperatures or shorter reaction times, if compared with other conventional methods like solid-state synthesis or nitrate method. The various advantages of adopting combustion synthesis as the prime method for the production of ABO_3 are

- Self-purifying feature due to the high temperatures involved,
- The possibility of obtaining products in the desired size and shape.
- Simple and cost effective,
- Homogeneous, very fine crystalline nanopowders without the intermediate decomposition and calcinations steps which other conventional synthesis routes would require
- Monophasic nanopowders at lower temperatures or shorter reaction times

1.6.1.1. Procedure

ABO_3 type materials were prepared by a novel combustion method using glycine as the fuel. The procedures adopted are

- Precursor was prepared in aqueous solution from metal nitrates and glycine. Solutions of 0.2MA $(NO_3)_3$ and 0.2MB $(NO_3)_3$ were prepared. As $A(NO_3)_3$ is insoluble in water, it was first dissolved in HNO_3.

• 50 ml of both the solutions was then properly mixed in a beaker.

• Glycine/nitrate ratio as taken as 0.1.The appropriate amount of glycine was then added to the above solution and the mixture was stirred until complete dissolution occurred.

• Then, the mixture was heated and evaporated on a hot plate with stirring till it became a dark viscous resin. Continuous heating leads to the auto-ignition of dried resin with the evolution of large quantities of gases.

• The brownish colour ash obtained after combustion was analyzed for perovskite-type ABO_3 phase.

• The whole process was over after 30 minute, but the time between the actual ignition and the end of the reaction was less than 20 second.

• After the combustion is over in chamber, it is further heated for 5-10 minutes to allow complete combustion of material.

• After cooling, it is taken out of chamber and grinding is done to achieve finer powder.

• After that, powder was calcined at 450^0C for 6 hours. The crystal structure of the synthesized powder was characterized.

1.6.2. Sol-gel Route

High purity multiferroic ABO_3 (ABO) powders were synthesized by sol – gel process using bismuth nitrate and iron nitrate as sources. The ABO powders annealed at 600^oC in nitrogen environment were mainly composed of a rhombohedral $BiFeO_3$ phase (R-phase) with a minor impurity phase of A_2O_3. A pure ABO R-phase has been obtained by leaching out the minor A_2O_3 phase using diluted nitric acid. A reversible phase transformation of the ABO R-phase has been detected at 836^oC by a differential thermal analysis. The powders of ABO R- phase exhibits a uniform feature with the particle size of 200 nm.

1.6.3. High energy ball milling Route

ABO_3 magneto electric compound had its synthesis optimized via high-energy ball milling technique for grain size reduction, as well as its sintering process, via

conventional route, for high density improvement. For homogeneous particle size we use this technique.

CHAPTER 2

LITRETURE REVIEW

Multiferroics materials have recently gained a considerable attention due to it multifunctional device application and underlying new physics. Among the class of multiferroics, $BiFeO_3$ is one of the widely investigated materials important materials due to it ferroelectric and magnetic transition temperature well above room temperature, which gives the possibility of RT multiferroics. In past years, large efforts have been made to get strong FE and FM polarization together. Researcher has done a considerable work on the processing and microstructral aspect on the properties of $BiFeO_3$. On other hand, the work also been carried out to substitute A site and B site by other transition metal ion and rare earth ions etc. Effect of substitution has been thoroughly investigated on the structural, electric and magnetic properties. In this chapter the important work carried out in last few years related to synthesis of $BiFeO_3$ and the substitution effect on the properties has been reviewed.

V. L. Mathe *et al.* 2002 [38] synthesized the $Bi_xLa_{1-x}FeO_3$ (x = 0.0, 0.20, 0.40, 0.60, 0.80) by solid-state reaction method. The single-phase formation of these compounds was found. The samples up to x = 0.60 were orthorhombic while the sample with x = 0.80 has changed to triclinic. The dielectric constant (ε) and dissipation factor (tan δ) were measured in the frequency range 100Hz to 1MHz at room temperature and as a function of temperature at certain fixed frequencies (1kHz, 10kHz, 100kHz, 1MHz). All the samples showed dielectric dispersion. The dielectric constant with temperature shows a broad peak; the peak temperature shifts with frequency which reflects the relaxor-type behavior. The peak above 600K in the measured temperature range corresponds to antiferromagnetic ordering temperature (Neel temperature). The broadness of the peak

changes with composition. The RT ac conductivity as well as ε are found to be maximum for the sample x = 0.20.

V. R. Palkar *et al.* 2004 [39] synthesized the $Bi_{0.9-x}Tb_xLa_{0.1}FeO_3$ powder samples ($0.0<x<0.30$) were developed by using a novel wet chemical route. The coexistence of ferroelectricity and magnetism was found. The samples found to exhibit high RT dielectric constant and magnetoelectric coupling.

A. K. Pradhan *et al.* 2005 [40] synthesized single phase $BiFeO_3$ by rapid liquid-phase sintering technique. The temperature-dependent magnetic measurement indicated RT antiferromagnetic behavior in $BiFeO_3$. Although saturated ferroelectric hysteresis loops were observed in single-phase $BiFeO_3$ ceramic synthesized at 880°C, the reduced polarization is found to be due to the high loss and low dielectric permittivity of the ceramic, which is caused by higher leakage current.

Jong Kuk Kim *et al.* 2005 [41] synthesized the high purity multiferroic $BiFeO_3$ (BFO) powders by sol–gel process using bismuth nitrate and iron nitrate as sources. The thermal annealing was carried out in N_2 atmosphere. The rhombohedral $BiFeO_3$ phase (R-phase) with a minor impurity phase of Bi_2O_3 is achieved. It is reported that pure BFO R-phase can be obtained by leaching out the minor Bi_2O_3 phase using diluted nitric acid. A reversible phase transformation of the BFO R-phase has been detected at 836^oC by a differential thermal analysis. The powder of BFO R-phase exhibits a uniform feature with the particle size of 200 nm. The dielectric constant of the BFO R-phase is measured to be ~15 in the frequency range of 10^4-10^6 Hz at room temperature.

D. H. Wang *et al.* 2006 [42] synthesized Ba substituted $BiFeO_3$ by solid-state reaction method. The substituted samples exhibit magnetism and ferroelectricity simultaneously at room temperature. The magnetoelectric coupling was evidenced by the increase of the dielectric constant with the increase of the applied magnetic field. For $Bi_{0.75}Ba_{0.25}FeO_3$

with H=8kOe, the values of [ε_r (H) − ε_r (0)/ε_r (0)] are 1.7% and 1% for 80 and 300 K, respectively.

Chang Fanggao *et al.* 2006 [43] synthesized $Bi_{1-x}Gd_xFe0_3$ (x = 0.0, 0.05, 0.10, 0.15, 0.20) ceramics by conventional solid state reaction method. Frequency dependence of dielectric properties of $Bi_{1-x}Gd_xFeO_3$ samples at room temperature was measured in a frequency range from 100 Hz to 1MHz using an HP4294A precision impedance analyzer. For all the samples studied, the dielectric constant and dielectric loss decreases with increasing frequency in the range between 100Hz and 1MHz, as can be expected from a typical orientational dielectric relaxation process. There is no indication of any dips over the whole frequency range studied, which is in direct contrast with that reported previously. It is found that both dielectric constant and dielectric loss are strongly dependent on the Gd^{3+} content. The effect of introducing Gd^{3+} is to increase the dielectric constant and to decrease the dielectric loss for slightly doped sample $Bi_{0.95}Gd_{0.05}Fe0_3$ the dielectric constant of the sample at 1 kHz reaches 600, six times bigger than that for pure $BiFeO_3$. Complicated dielectric behaviors are observed at higher doping levels. Furthermore, the substitution of rare earth Gd for Bi helps to eliminate the impurity phases in $BiFeO_3$ ceramics. There is strong evidence that both lattice constants *a* and *c* of the unit cell become smaller as the Gd^{3+} content is increased. The dielectric constant and loss and their frequency responses can be varied dramatically by substitution of Gd.

Shan-Tao Zhang *et al.* 2006 [44] synthesized the single-phase, insulating $Bi_{1-x}La_xFeO_3$ ($B_{1-x}La_xFO_3$, x=0.05, 0.10, 0.15, 0.20, 0.30, and 0.40) ceramics were prepared. The phase transition from rhombohedral to orthorhombic phase was observed near x=0.30. It is found that the phase transition destructs the spin cycloid of $BiFeO_3$ (BFO), and therefore, releases the locked magnetization and enhances magnetoelectric interaction. As a result, improved multiferroic properties of the BLFO (x=0.30) ceramics with remnant polarization and magnetization of 22.4μC/cm2 and 0.041emu/g, respectively, were recorded.

G. L. Yuan *et al.* 2006 [45] synthesized single-phase $Bi_{1-x}Nd_xFeO_3$ (x=0.0, 0.15, 0.175, 0.20) multiferroic ceramics were prepared to study the effects of Nd substitution on their crystal structure and ferroelectromagnetic behavior. Rietveld refinement of x-ray diffraction data showed a continual transformation of crystal structure from the rhombohedral structure of $BiFeO_3$ to a triclinic structure in $Bi_{1-x}Nd_xFO_3$ (x=0.05–0.15) and a pseudo tetragonal structure in $Bi_{1-x}Nd_xFO_3$ (x=0.175–0.20). Ferroelectromagnetic measurements revealed the existence of ferroelectricity with remnant polarization of ~9μC/cm^2 in $Bi_{1-x}Nd_xFO_3$ (x=0.0–0.175), paraelectricity in $Bi_{1-x}Nd_xFO_3$ (x=0.20), and weak ferromagnetism with remnant magnetizations of 0.07–0.227emu/g in $Bi_{1-x}Nd_xFO_3$ (x=0.15-0.20). Magnetoelectric coupling was obvious in $Bi_{1-x}Nd_xFO_3$ (x=0.15–0.175) near the Neel temperature of ~380°C. This group further polarized the samples and piezo and pyroelectric effects on substituted samples were investigated [46]. The success in polarizing the ceramics originates from low electrical conductivities controlled predominantly by the Poole-Frenkel conduction mechanism. Limited internal traps due to reduced oxygen vacancies in the ceramics result in sufficiently low leakage current densities of <30mA/m^2 even at a high electric field of 145kV/cm. The piezoelectric d_{33} coefficients of the ceramics before and after annealing at 550°C for 4 hours are measured to be ~28 and ~24pC/N, respectively. These values are higher than those of most major lead-free high-temperature piezoelectric ceramics. In the same year, the group also investigated the effect Sm substitution on structural and multiferroic properties [47]. The triclinic structure with P1 space group was confirmed in the ceramics by refining the x-ray diffraction pattern. Large piezoelectric d_{33} coefficient of 29pC/N, together with high remnant polarization of 15.09μC/cm^2, was measured at room temperature, suggesting the existence of long-range ferroelectric order on a macroscopic scale. The observed small remnant magnetization of 0.071emu/g at room temperature as a result of the collapse of the space-modulated spin structure indicated the presence of long-range canted antiferromagnetic order on a macroscopic scale. The coexistence of the long-range ferroelectric and canted antiferromagnetic orders allowed the magnetoelectric effect

below the antiferromagnetic Neel temperature of 265°C near which magnetoelectric coupling was obvious.

Deepti Kothari *et al.* 2007 [48] reported that Ca^{2+} doping at Bi-site results in the release of weak ferromagnetism in $BiFeO_3$. Structural transformation from rhombohedral to triclinic is observed with 10% Ca doping. Raman measurements show the presence of oxygen vacancies with Ca doping and no evidence of either intermediate valence or the tetravalence of iron is observed from Mössbauer measurements. No significant change in Neel temperature is observed with Ca doping. The observed weak ferromagnetism and ferroelectric nature at room temperature indicates the multiferroic nature of $Bi_{1-x}Ca_xFeO_3$ samples.

V. A. Khomchenko *et al.* 2007 [49] sintered the $Bi_{1-x}A_xFeO_3$ ceramics (A=Ca, Sr, Pb) by conventional mixed oxide route. The crystallographic structure of all samples is characterized by the rhombohedral symmetry (space group R3c). The existence of switchable ferroelectric polarization is verified by piezoresponse force microscopy. Magnetic properties of Ca and Sr-doped ceramics are found to reproduce the antiferromagnetic behavior of undoped $BiFeO_3$ without any enhancement of the magnetization. On the contrary, Pb-doped compound demonstrates appearance of a weak ferromagnetism. It is thus shown that Pb doping of $BiFeO_3$ is a promising way for preparing multiferroic materials.

S. R. Das *et al.* 2007 [50] investigated the magnetic and the electrical properties in lanthanum (La)-modified bismuth ferrite ($Bi_{1-x}La_xFeO_3$, x=0.05, 0.1, 0.15, and 0.2) and compared with undoped bismuth ferrite ($BiFeO_3$). The presence of a small secondary phase of $BiFeO_3$ (arises due to excess Bi_2O_3) was removed on La substitution at the Bi site, as observed in x-ray diffraction (XRD). The effect of La substitution on dielectric constant, loss tangent, and remnant polarization of the samples was studied in a wide range of temperature (77K–400K) and frequency (1kHz–1MHz). The variation of

magnetization, coercive field, with temperature (2K–300K) and La concentration were investigated. These changes in the magnetic parameters with La doping along with those of the electron magnetic resonance parameters measured at 300 K and 9.28GHz are understood in terms of increase in the magnetic anisotropy and magnetization. These results also show that stabilization of crystal structure and non-uniformity in spin cycloid structure by La substitution enhances the multiferroic properties of $BiFeO_3$.

W. N. Su *et al.* 2007 [51] synthesized the $BiFeO_3$ ceramics by sol-gel method (BFO-1) and high-pressure synthesis (BFO-2). X-ray diffraction showed that these ceramics are almost of single phase. It is difficult to observe a ferroelectric loop of BFO-1 even at an electric field of 6kV/cm. Compared to BFO-1, the high-pressure synthesized one has higher resistivity, higher density, and better crystallization. Under an applied electric field of 120kV/cm, the values of remnant polarization and the coercive field are 46μC/cm^2 and 73kV/cm, respectively. At room temperature, a magnetic hysteresis loop with enhanced magnetization was observed in BFO-2.

Z. Yan *et al.* 2007 [52] prepared Yb-doped bismuth iron oxide ceramics $Bi_{1-x}Yb_xFeO_3$, with ($0.0<x<0.20$) by rapid liquid phase sintering method and investigated the material's structures and electrical properties. The x-ray diffraction measurements showed that the doping of Yb has induced noticeable lattice distortion in the ceramics, and a largest distortion was observed when the concentration of Yb was 15%. By doping electrical resistivity, ferroelectric and dielectric properties of the ceramics were improved. Among all samples, $BiFeO_3$ doped with 15% Yb was found to have the smallest leakage current density (10−7 A/cm^2) and the largest remnant polarization (8.5μC/cm^2).

M. Thrall *et al.* 2008 [53] synthesized the multiferroic $BiFeO_3$ by using both vacuum and argon atmospheres. The synchrotron X-ray powder diffraction investigation on pressed pellets of the starting powders of Bi_2O_3 and Fe_2O_3 were carried out upto the final formation of $BiFeO_3$. The difference in the transformation temperature of monoclinic

Bi_2O_3 to cubic Bi_2O_3 was found to be 650 and 700^oC when samples were sintered in a vacuum and argon environments, respectively. It was found that this reaction was 75% complete before the multiferroic product began to form. In both cases it was found that the quantity of Fe_2O_3 was unaffected by increasing temperature until after the transition of monoclinic to cubic Bi_2O_3 had reached its maximum value. After this transition the quantities of cubic Bi_2O_3 and Fe_2O_3 were found to decrease at very similar rates yielding the final $BiFeO_3$ structure. An SEM study of the bulk microstructure of the $BiFeO_3$ product showed a poor densification due to incomplete reactions between the remaining Bi_2O_3 and Fe_2O_3.

V. A. Khomchenko *et al.* 2008 [54] studied the room-temperature crystal structure, local ferroelectric, and magnetic properties of the $Bi_{1-x}Gd_xFeO_3$ (x=0.10, 0.20, 0.30) polycrystalline samples by x-ray diffraction, piezoresponse force microscopy, and magnetometry techniques. Performed measurements have revealed a sequence of the composition-driven structural phase transitions R3c→$Pn2_1a$ (occurs at x=0.10) and $Pn2_1a$→Pnma (takes place within the concentrational range of 0.20<x<0.30). The latter structural transformation is attributed to the substitution-induced suppression of the polar displacements. Gd substitution has been shown to effectively induce the appearance of the spontaneous magnetization, thus indicating a promising way for improving multiferroic properties

R.K. Mishra *et al.* 2008 [55] synthesized the polycrystalline samples of $Bi_{1-x}Nd_xFeO_3$ (BNFO) with x = 0.0, 0.05, 0.10, and 0.15 by a chemical route. A systematic change in crystal structure from rhombohedral to tetragonal on increasing Nd substitution was observed. The reduction of low frequency dispersion in permittivity and loss pattern due to Nd substitution in $BiFeO_3$ (BFO) was observed in its dielectric response curve. The loss tangent (tanδ) was found to be reduced on increased Nd concentration in BNFO. Dielectric anomaly near the reported Neel temperature of BFO and peaks in all the BNFO samples were observed in the permittivity vs. temperature graph. Significant opening in

the room temperature M–H loop was observed on Nd substitution, which was more prominent for higher concentration of Nd.

V. Raghavendra Reddy *et al.* 2009 [56] reported that room temperature spontaneous magnetization and dielectric anomaly at Neel temperature are observed in 15% Eu doped bismuth ferrite indicating the multiferroic nature of the sample. With 15% Eu doping structural transformation from rhombohedral to triclinic is observed. Fe^{3+} and Eu^{3+} oxidation states are observed from ^{57}Fe and ^{151}Eu Mossbauer measurements, respectively. The high field ^{57}Fe Mossbauer spectrum in longitudinal geometry shows an enhancement in the intensity of lines corresponding to $\triangle m=0$ transitions, i.e., second and fifth lines in six line pattern. This observation suggests that the origin of spontaneous magnetization is due to weak ferromagnetism.

V.A. Khomchenko *et al.* 2009 [57] studied the crystal structure, magnetic and local ferroelectric properties of polycrystalline $Bi_{1-x}Gd_xFeO_3$ (x = 0.10, 0.20, 0.30) samples at room temperature. Gadolinium substitution was found to induce a polar-to-polar R3c $Pn2_1a$ structural phase transition at x=0.10. Increasing the content of the substituting element suppressed the spontaneous polarization in $Bi_{1-x}Gd_xFeO_3$, resulting in a ferroelectric–paraelectric $Pn2_1a$ to Pnma phase transition up to the level $0.20 < x < 0.30$. The substitution caused the appearance of a weak ferromagnetic moment.

A.Z. Simoesa *et al.* 2009 [58] Lanthanum-modified bismuth ferrite ceramics, $Bi_{1-x}La_xFeO_3$ (BLFO), with x ranging from 0.0 to 0.30 were obtained using a polymeric precursor solution. Orthorhombicity of the system raised with the increase of lanthanum content in the BFO crystal lattice. No secondary phases were reported after lanthanum addition. A homogeneous size distribution of BFO powders was evidenced by scanning electron microscopy. Increasing lanthanum content leads to lower leakage current density and superior ferroelectric hysteresis loops at room temperature.

Mansour Al-Haj *et al.* 2010 [59**]** synthesis the multiferroic compounds $Bi_{0.9}Sm_{0.1}FeO_3$, $Bi_{0.9}Gd_{0.1}FeO_3$, $Bi_{0.9}Ca_{0.1}FeO_3$, $Bi_{0.9}Sm_{0.05}Ca_{0.05}FeO_3$, and $Bi_{0.9}Gd_{0.05}Ca_{0.05}FeO_3$ by the conventional ceramic method and were characterized by X-ray diffraction, vibrating sample magnetometry, and differential scanning calorimetry. The compounds were found to have the rhombohedral perovskite-like structure, accompanied by a small residual $Bi_2Fe_4O_9$ impurity phase. Magnetic hysteresis loops with enhanced remnant magnetization and coercive field were obtained for the Gd-containing compounds. The improvement of magnetic behavior of the Gd-containing compounds is thought to arise mainly from the partial suppression of the spiral spin structure and the stronger interaction between magnetic ions. The magnetic transition temperatures of the compounds were found to be in the range 300^{o}C-310°C.

Yi Dua *et al.* 2010 [60] synthesized the multiferroic $Bi_{1-x}La_xFeO_3$ (x = 0.0, 0.10, 0.20, 0.30) micro-particles by a hydrothermal technique. All the samples were phase pure crystallizing in a perovskite structure with a space group of R3c. XRD refinement revealed that the lattice parameters increased along with increase of La content, while the Fe–O octahedral became more distorted. It was found that the morphologies of as-obtained micron-sized particles turned from spheroidal to octahedral according to different doping levels. The dielectric constant of $Bi_{1-x}La_xFeO_3$ sample increased after La doping, and reached the largest value for the sample of x = 0.20, both in low and high frequency range at room temperature. All the as-prepared samples exhibited magnetic moments starting above room temperature. It was found that the magnetic moment was significantly enhanced from 0.264 emu/g of $BiFeO_3$ to 0.658 emu/g of $Bi_{0.9}La_{0.1}FeO_3$ in a field of 3T at 77K. Both enhancements of ferromagnetic and dielectric properties were explained on the basis of changes of lattice parameters and Fe–O bond lengths caused by lanthanum substitution.

Xiaolong Yan *et al.* 2010 [61] synthesis the $Bi_{1-x}La_xFeO_3$ (BLFO, x = 0.0–0.20) crystallites by the hydrothermal route. X-ray diffraction results indicate that pure BLFO crystallites could be obtained for $x \leq 0.10$, and the phase purity was sensitive to the PH value of precursor solutions. Transmission electron microscope observation reveals that needle like BLFO crystallites were formed for x = 0.10. The Neel temperature of BLFO crystallites for x = 0.1 shifts upwards, whereas the Curie temperature shifts downwards, compared with those of BFO crystallites without La substitution. Weak ferromagnetic property of BLFO crystallites was induced and enhanced with increasing the La content.

V.A. Khomchenko *et al.* 2010 [62] studied the crystal structure and multiferroic properties of polycrystalline $Bi_{1-x}Sm_xFeO_3$ (0.16 <x <6 0.20) samples was performed by X-ray diffraction, piezoresponse force microscopy and SQUID-magnetometry techniques. It was reported that increasing samarium content induced a polar-to-nonpolar phase transition near x=0.2. Within the polar region, a rhombohedral and two orthorhombic modifications of $Bi_{1-x}Sm_xFeO_3$ were found. It was shown that samarium substitution resulted in the appearance of spontaneous magnetization, which was significantly enhanced upon the composition-driven transition from a rhombohedral to an orthorhombic phase.

CHAPTER- 3

EXEPERIMENTS PROCEDURE

The polycrystalline $Bi_{1-x}Gd_xFeO_3$ (x=0.0, 0.05, 0.10, 0.15, 0.20) were prepared by high energy ball milling followed by thermal annealing. The raw materials used for the experiments were Bi_2O_3 (Loba Chem), Gd_2O_3 (Loba Chem), and Fe_2O_3 (Sigma Aldrich) with 99% purity. The raw materials were weighed in their stoichiometric composition and then mixed manually by using pestle & mortar for half an hour; further the wet mixing were carried for 3 hours using planetary ball mill in acetone media. The RPM and ball to charge ratio were 60 and 2:1 respectively. After mixing the excess acetone were drained and the powder were dried in normal atmosphere. The dried powder was further submitted to high energy ball milling in tungsten carbide zar for 10 hours. The RPM were fixed to 250. The ball to charge ratio was 10:1 (for 1 gram powder 10 gram ball is required). To understand the phase formation temperature the as-milled powder were studied by differential thermal analysis (DTA) and thermogravimetric analysis technique (TGA) were carried out by using the instruments Perkin Elmer (Pyris Diamond TG/DTA). Thermal annealing of the un-doped milled sample were carried out between the temperature 750^{o}C to 900^{o}C, in tubular furnace at ambient atmosphere. The holding time were fixed to one hour. The doped sample was thermally annealed at optimal temperature for one hour. Phase identification of the annealed powders was carried out by X-ray diffraction instruments X'Pert Pro-Panlytical. FTIR of the powders were carried out by spectrum BX II instruments (Perkin Elmer). Further the powder was pressed into pellets of 10 mm diameter die under 10 ton/cm^2 pressure using hydraulic press. The pressed pellets were sintered 875^{o}C temperature for four hours. For dielectric and P-E loop measurements the sintered pellets were coated on both sides by Ag paste. The dielectric measurements were carried out by the instruments LCR meter Agilent 4284A (frequency range 20Hz to 1MHz) and the P-E loop of the pallets were carried out by the

instruments ALIGENT 4284A The scanning electron microscopy the samples were carried out using SEM model JEOL JSEM 6510VL. Before SEM the samples were made conduction by sputtering of Ag layer of thickness 10 nm approximately. Fig. 3.1 shows the flow diagram of the processing and characterization of the samples.

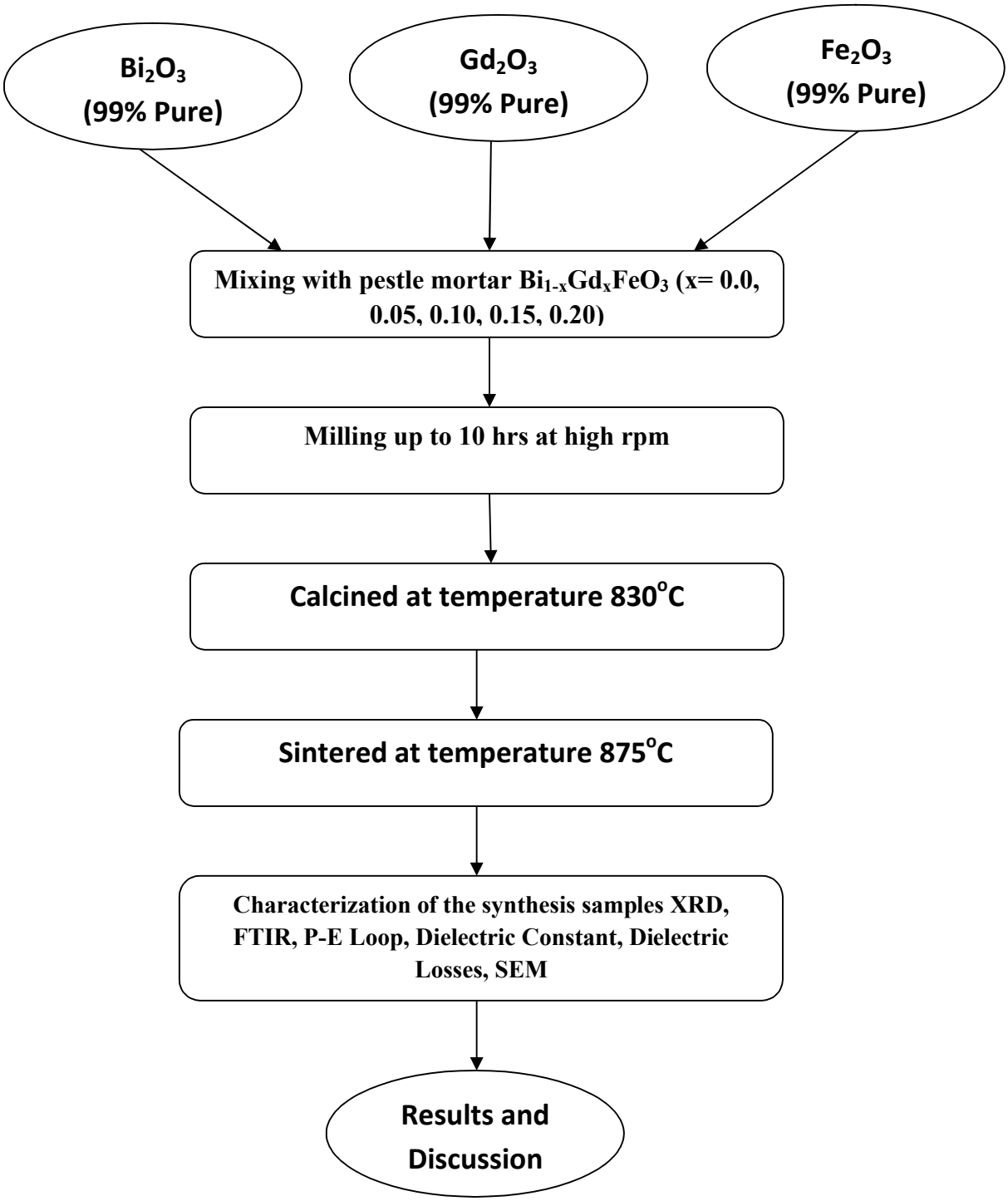

Fig3.1: Flow chart of the experimental work

CHAPTER 4

RESULTS AND DISCUSSION

4.1. Thermal Analysis of the milling powder

The thermal analysis of the milled samples was carried out using DTA and TGA. Fig.4.1 shows the TGA/DTA of the milled (Bi_2O_3 + Fe_2O_3) powder. The DTA of the synthesis sample shows the small endothermic peaks at the temperature 827^oC, 859^oC, and 948^oC. These peak may be arises due to different phase formation occurs at different temperature, which will further confirmed by X-ray studies. The corresponding TGA graph shows increase in the weight within the measured temperature range. In TGA, there are two maxima at the temperature 920^oC and 959^oC indicating the phase formation in the sample. From the DTA curve it is evident that phase formation occurred at 827^oC, however, there are also few phase which form below 827^oC also but their evidence are not noted in the curves. This may be due to faster heating rate (10^oC/min).

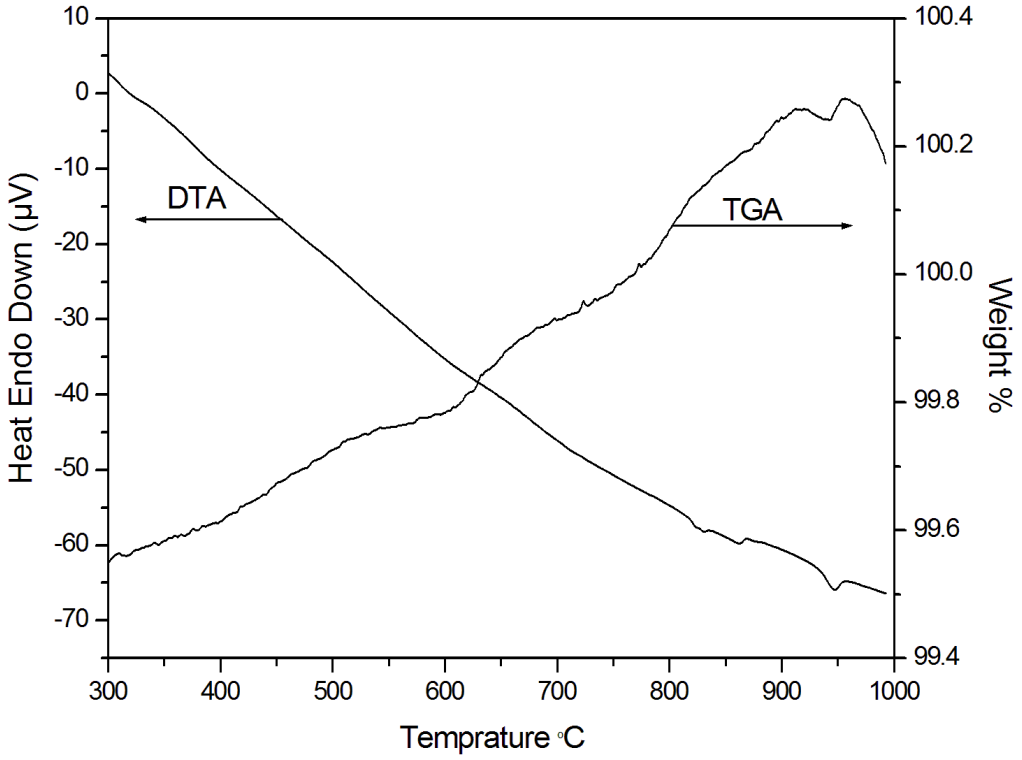

Figure 4.1: DTA/TGA curve of the milled powder

4.2. X-ray diffraction Studies

Fig 4.2 (i) (a), (b) shows the X-ray diffraction pattern of the as received Fe_2O_3, and Bi_2O_3 powder. Both are single phase powder no impurity phase was found. Fig. 4.2 (i) (c) shows the XRD pattern of high energy ball milled powder (Fe_2O_3 + Bi_2O_3) for 10 hours. It is evident that in milled sample peak broadening takes place, which indicate that particle size has been reduce. By Scherrer Equation the particle size of Bi_2O_3, particle size of Fe_2O_3, and the particle size of milled sample are 23nm, 20nm, and 13nm respectively. After milling $Bi_{36}Fe_2O_{57}$ (JCPDS 42-0181) phase is formed along with the residual Fe_2O_3 are found.

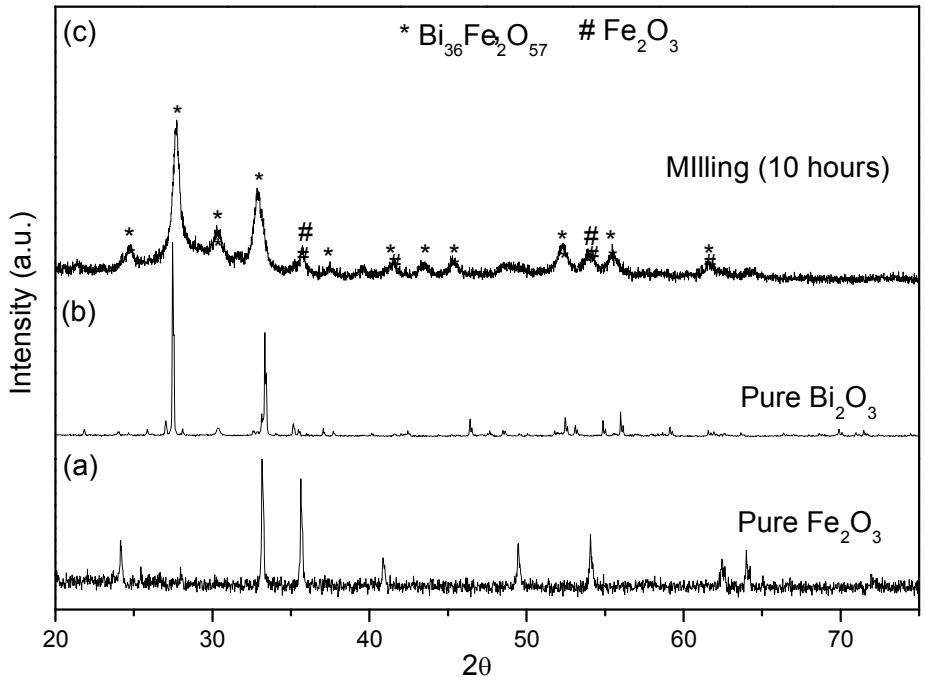

Figure 4.2 (i): X-ray diffraction pattern of (a) Fe_2O_3 (b) Bi_2O_3 (c) milled (Fe_2O_3 + Bi_2O_3) powder for 10 hours

The X-ray diffraction patterns of milled powder calcined at different temperatures are shown in fig 4.2 (ii). Samples calcined at 750^{o}C shows $Bi_2Fe_4O_9$ (JCPDS 20-0836) phase along with formation of $BiFeO_3$ (JCPDS 14-0181) phase. With increasing temperature to 800^{o}C the intensity of $BiFeO_3$ phase increases with two impurity phase of $Bi_2Fe_4O_9$ and $Bi_{25}FeO_{40}$ (JCPDS 46-0416) are found. Further increasing the temperature to 830^{o}C Single phase BiFO3 formed, however very small amount of residual phase are present. The results are in similar lines as reported before [63]. From the fig 4.2 (ii), at the temperature 830^{o}C the maximum purity phase of $BiFeO_3$ (JCPDS 14-0181) is formed and the residual impurity phases are $Bi_2Fe_4O_9$ and $Bi_{25}FeO_{40}$ are formed. At the calcine

temperature 850°C and 900°C the maximum impurity phase of $Bi_2Fe_4O_9$ is formed and emerges out at the cost of $BiFeO_3$ phase.

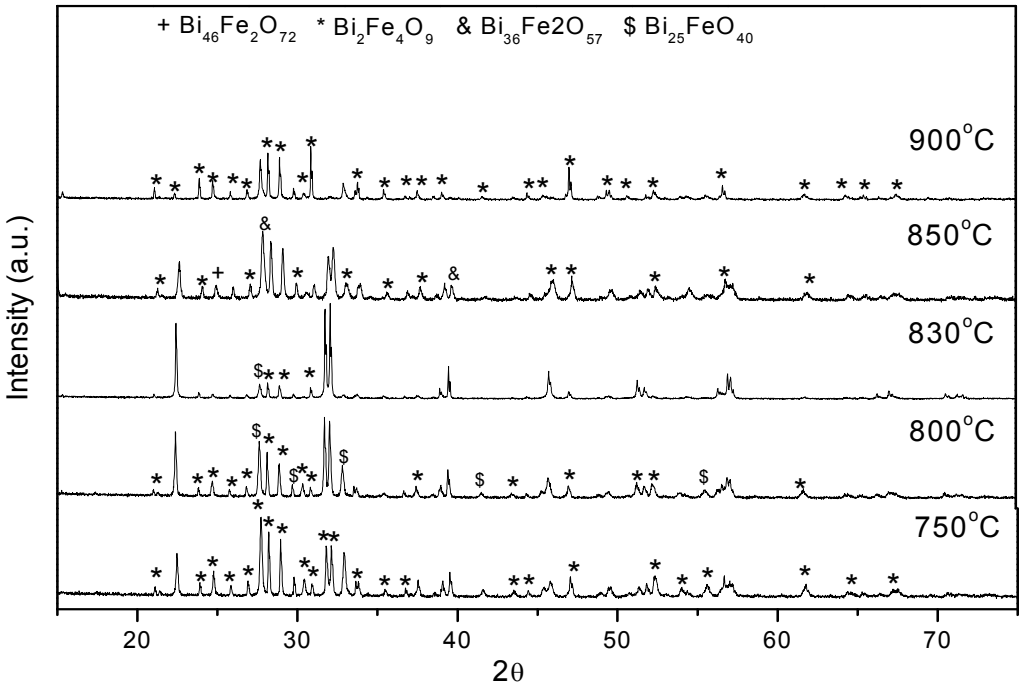

Figure4.2 (ii): X-ray diffraction pattern of $BiFeO_3$ after calcined at different temperature range

The X-ray diffraction pattern of $Bi_{1-x}Gd_xFeO_3$ (x=0.0, 0.05, 0.10, 0.15, 0.20) calcined at 830°C are shown in fig 4.2(iii). With increasing the Gd (x=0.05) amount it is evident that impurity phases decreased and pure $BiFeO_3$ without any impurity phase has been found at the Gd concentration at x=0.10. As we increase the concentration of Gd upto x=0.15, the second phase $Bi_2Fe_4O_9$ is formed. At x=0.2 phase small amount of $Bi_{36}Fe_2O_{57}$ (JCPDS 42-0181) phase is also formed along with $Bi_2Fe_4O_9$.

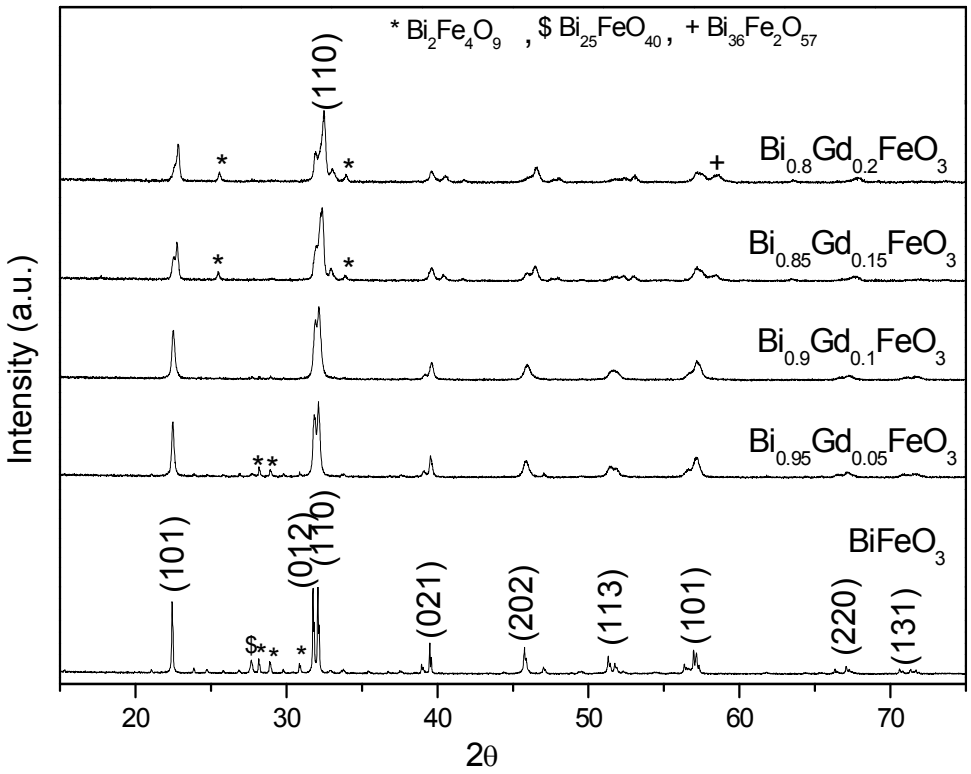

Figure 4.2(iii): X-ray diffraction pattern of $Bi_{1-x}Gd_xFeO_3$ (x=0.05, 0.10, 0.15, 0.20)

Fig.4.2 (iv) showes the variation in crystalline size with the Gd substitution. The particle size of undoped $BiFeO_3$ is 33.79nm and after substitution of Gd the particle size reduce abruptly up to 22.51nm at x =0.05 and it is almost constant upto the dopand level x=0.20.

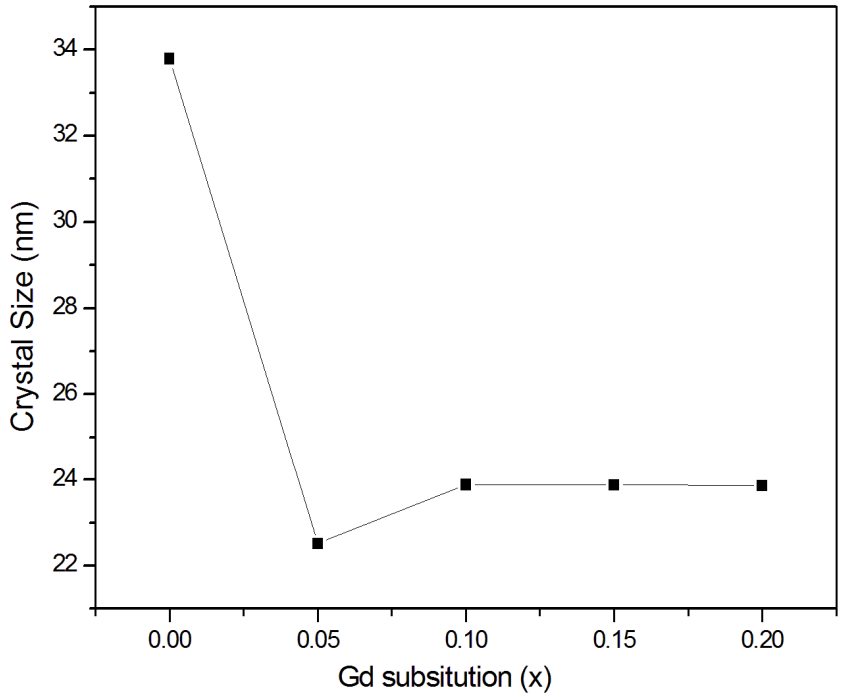

Figure4.2 (iv): Variation in the crystal size with the Gd substitution

4.3. FTIR spectrum of $Bi_{1-x}Gd_xFeO_3$ (x=0.0, 0.05, 0.1, 0.15, and 0.2)

The FTIR spectrum of undoped and doped synthesized samples $Bi_{1-x}Gd_xFeO_3$ x=0.0, 0.05, 0.10, 0.15, 0.20) carried out using spectrum BX II instruments (Perkin Elmer) in the range 400-2000 cm^{-1} as presented in the fig.4.3 (i) and fig.4.3 (ii). We found the constant refection in the region 400 to 500cm^{-1} in Fe-O bond of Fe_2O_3 up to 850^oC. At higher temperature up to 900^oC this peaks eventually disappears indicating the diffusion the of Fe-O stretch. Only one stretch was found in the region 400 to 525cm^{-1} corresponds to the presents of metal oxide bonds at lower doping concentration. However as the concentration of the doped was increased sharp reflection at 442cm^{-1} & 439cm^{-1} has been observed indicting the presence of Fe–O bond (stretching & bending) in this

range. It is quite evident from the fig.4.3 (ii) that these is no extra peaks unreacted material appeared indicating the substitution of doped impurity in the valence site.

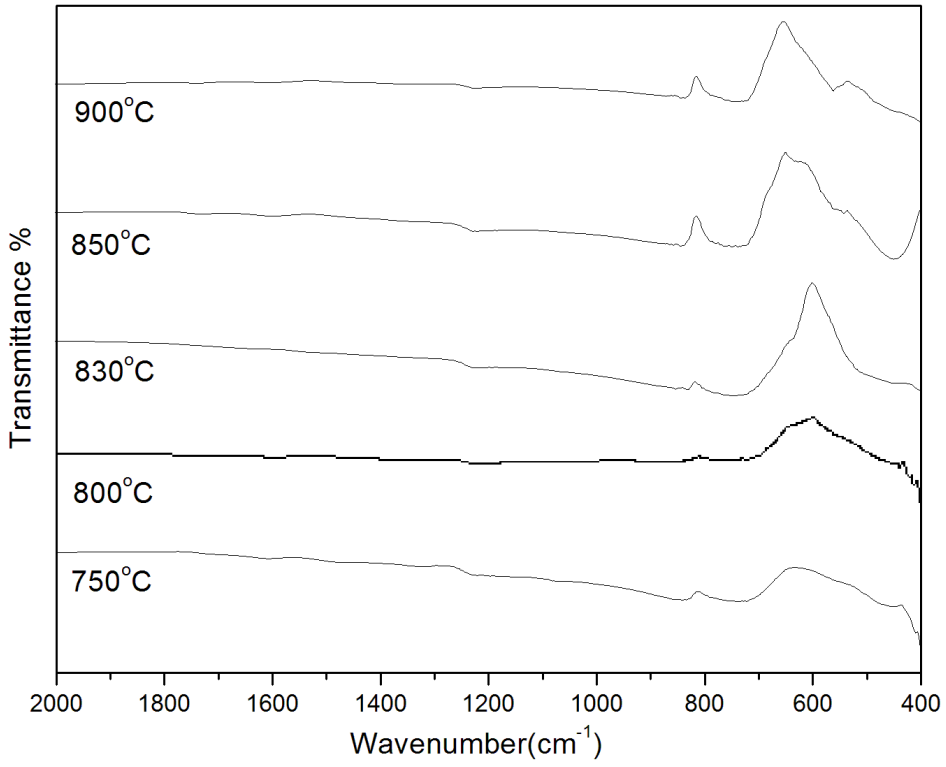

Figure 4.3 (i): FTIR spectrum of $BiFeO_3$ calcined at different temperature

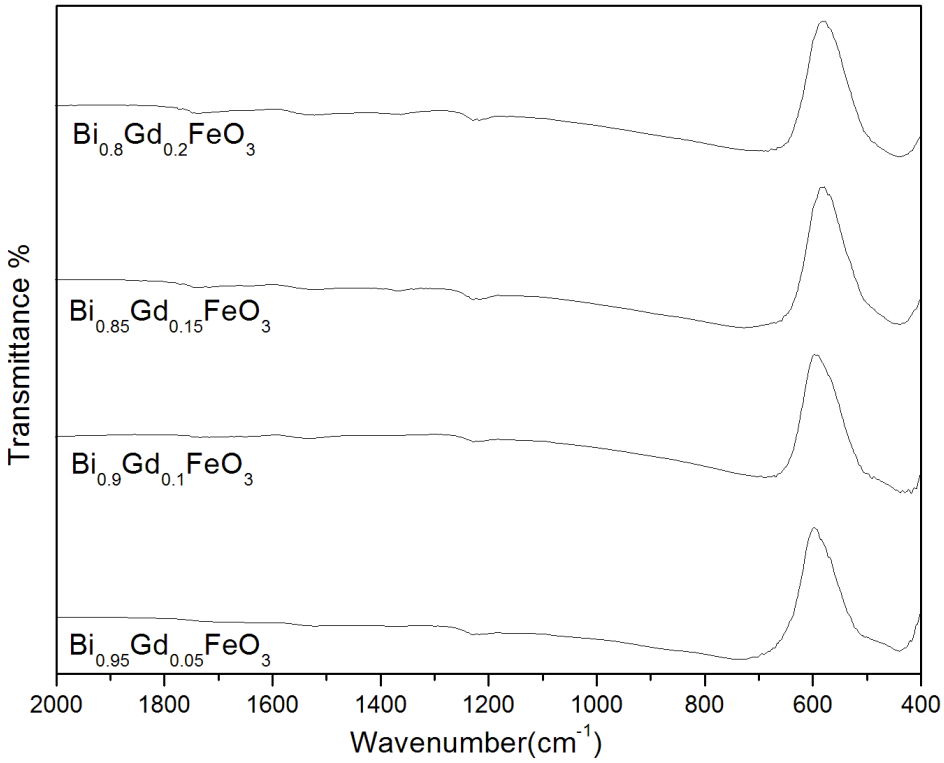

Figure 4.3 (ii): FTIR spectrum of $Bi_{1-x}Gd_xFeO_3$ (x=0.05, 0.10, 0.15, and 0.20)

4.4. P-E Loop measurements

The polarization of the doped samples $Bi_{1-x}Gd_xFeO_3$ (x=0.05, 0.10, 0.15, and 0.20) was carried out with the help of instrument P-E loop tracer at the room temperature as shown in fig4.4 (i). The maximum field is applied up to 55kv/cm. There is no saturation in the samples due to leakage current [64, 65]. The remnant polarization P_r and maximum polarization Pm is a function of Gd concentration x as shown in table4.4 (i).

Fig.4.4 (ii) shows as we increase the concentration of Gd (x=0.05, 0.10, 0.15, 0.20) the polarization increase up to Gd (x=0.10) and then polarization decrease as we increase concentration of Gd (x=0.15, 0.20). It is clear from the fig4.4 (ii) the polarization

of the sample $Bi_{0.9}Gd_{0.1}FeO_3$ is high as compare to other samples. The corecivity and the remnant polarization increase upto the x=0.15 and further it is decrease upto the level x=0.20.

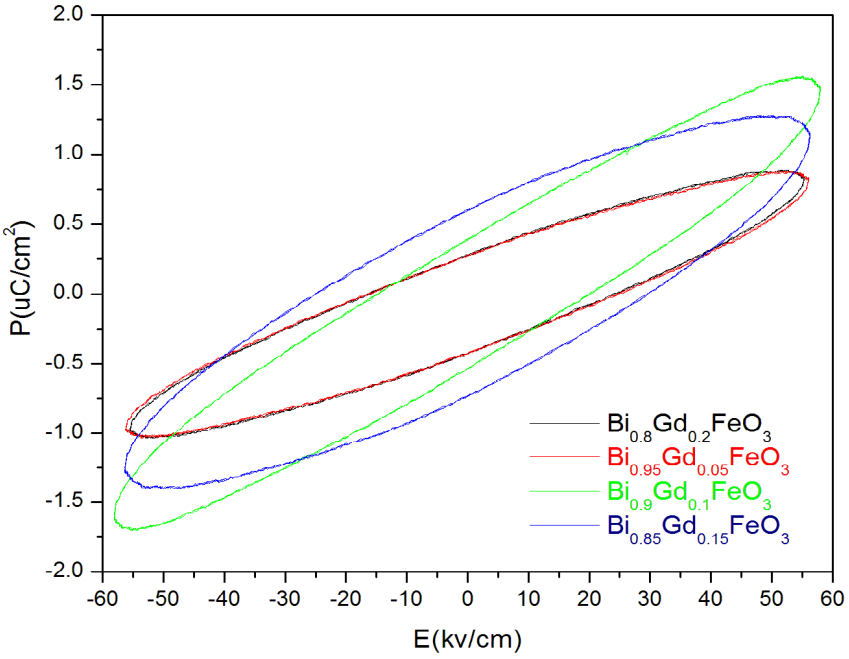

Figure 4.4(i): P-E Loop of the $Bi_{1-x}Gd_xFeO_3$ (x=0.0, 0.05, 0.10, 0.15, 0.20)

Table 4.4(i): polarization measurements of the Gd doped in the $Bi_{1-x}Gd_xFeO_3$ samples

Name of the Sample	Coercivity (kv/cm)	Remnant Polarization Pr ($\mu C/cm^2$)	Polarization Pm($\mu C/cm^2$)
$Bi_{0.95}Gd_{0.05}FeO_3$	8.081	0.364	0.651
$Bi_{0.90}Gd_{0.1}FeO_3$	17.386	0.461	1.630
$Bi_{0.85}Gd_{0.15}FeO_3$	27.246	0.675	1.342
$Bi_{0.8}Gd_{0.2}FeO_3$	20.381	0.354	0.961

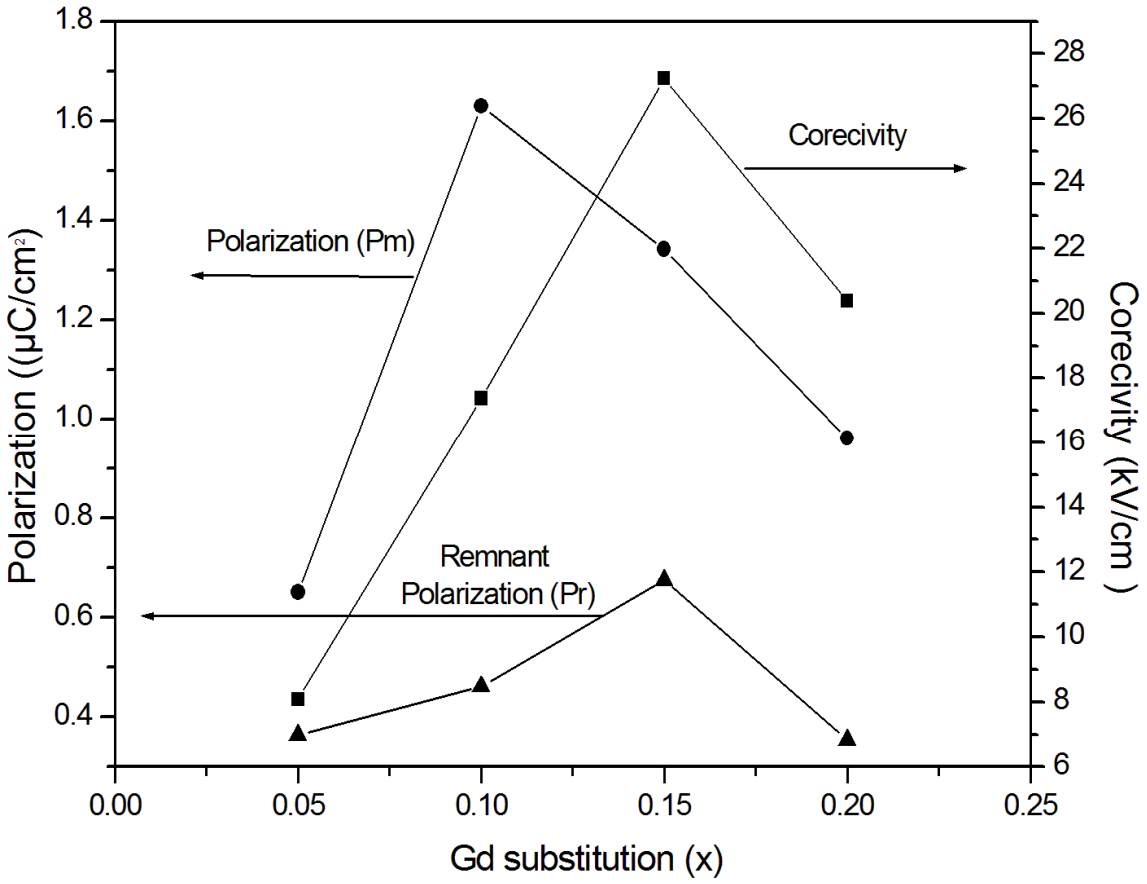

Figure 4.4 (ii): Polarization behavior of the sample with Gd substitution

4.5. Measurements of Dielectric Properties

Fig. 4.5 shows the dielectric constant measurements with respect to frequency in the range of 20Hz to 1MHz at room temperature for the composition $Bi_{1-x}Gd_xFeO_3$ (x=0.0, 0.05, 0.10, 0.15, and 0.20) using LCR meter. It was observed that the value of dielectric constant was found to be higher for the composition $Bi_{1-x}Gd_xFeO_3$ (x=0.1) attribute to the pure phase. The obtained value of the dielectric constant value measured at room temperature for the pure phase composition is comparable with the other reported values [64]. For all samples it is seemed that the value of dielectric constant was high at lower frequency and decrease as the frequency increased as expected and was nearly

constant at higher frequency. This property can be understood by the space charge relaxation phenomena where at the low frequency the space charge able to follow the frequency but at the higher frequency the space charge may have not have time to undergo relaxation [65]. The drastically change in the dielectric constant as increase the composition of Gd (x=0.05, 0.10, 0.15, 0.20) as compared to the pure sample $BiFeO_3$.

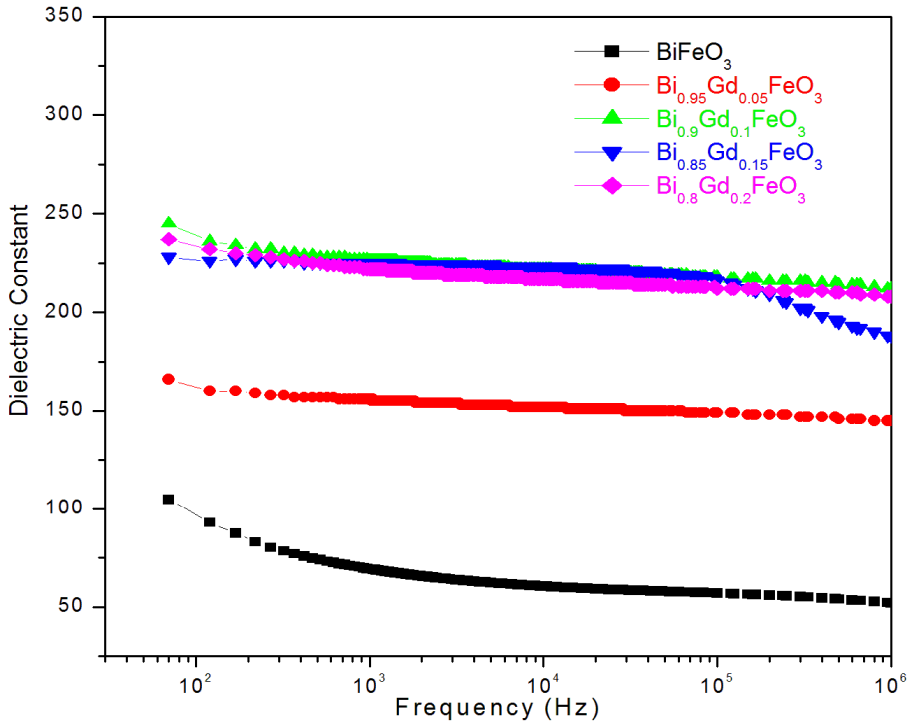

Figure 4.5 (i): Dielectric constant in $Bi_{1-x}Gd_xFeO_3$ (x=0.05, 0.10, 0.15, and 0.20)

Fig4.5 (ii) shows the dielectric losses measurements with respect to frequency in the range of 20Hz to 1MHz for the composition $Bi_{1-x}Gd_xFeO_3$ (x=0.0, 0.05, 0.10, 0.15, 0.2) at room temperature using LCR meter. It was observed that the value of dielectric losses was found to be higher for the composition of pure synthesis $BiFeO_3$. The obtained value of the dielectric losses value measured at room temperature for the pure phase

composition is comparable with the other reported values. For all samples it is seemed that the value of dielectric losses was high at lower frequency and decrease as the frequency increased as expected in the pure $BiFeO_3$ and was nearly constant at higher frequency. In the composition at Gd (x=0.15) the relaxation peaks was observed it is due to dielectric resonance, which is at higher frequency when the dipole relaxation are at right rate for maximum power dissipation. The sudden change in the dielectric losses as we doped Gd (x=0.05, 0.10, 0.15, 0.20) as compared to the pure sample $BiFeO_3$. The dielectric losses were minimum and constant of the sample $Bi_{1-x}Gd_xFeO_3$ (x=0.05, 0.10, 0.15, 0.20) with respect to frequency range 20Hz to 1MHz. It is shows in the fig.4.5 (ii) that the loss is minimum in the sample $Bi_{0.9}Gd_{0.1}FeO_3$ as compared to other samples

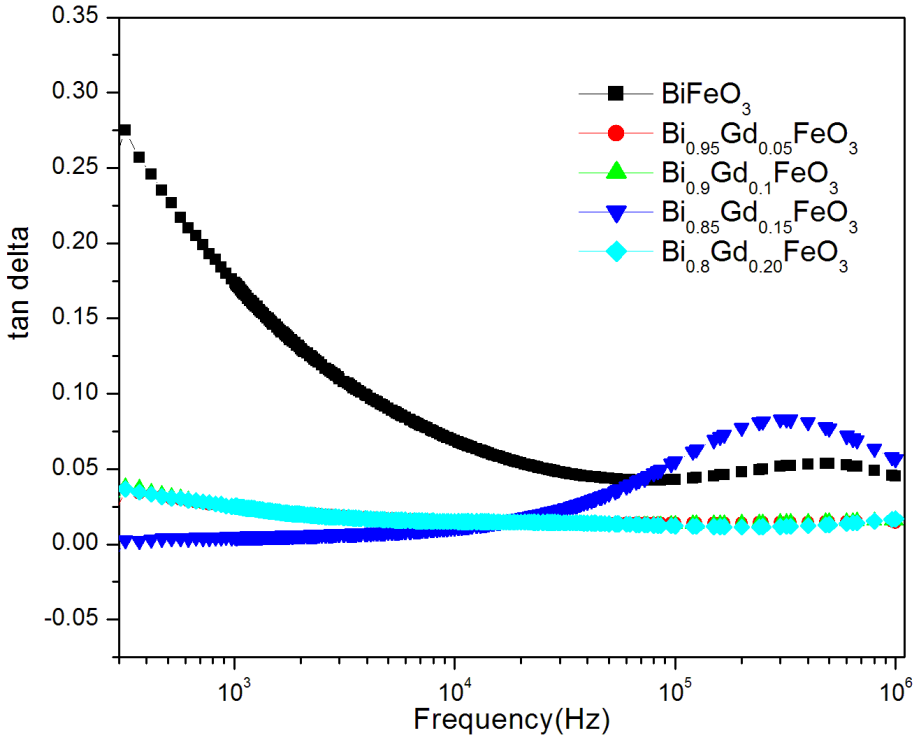

Figure 4.5 (ii): Dielectric losses in $Bi_{1-x}Gd_xFeO_3$ (x=0.05, 0.10, 0.15, and 0.20)

4.6. SEM image of the pure $Bi_{1-x}Gd_xFeO_3$ (x=0.0, 0.10, 0.20)

Fig.4.6 (i), 4.6(ii), 4.6(iii) shows the scanning electron micrographs of sintered pellets of $BiFeO_3$, $Bi_{0.9}Gd_{0.1}FeO_3$ and $Bi_{0.8}Gd_{0.2}FeO_3$ sample at different magnification. It is evident from the entire figure that the grain of pure $BiFeO_3$ sample is large and rectangular in shape. The grain size was in the range of 5-7 μm. As we increased the concentration of Gd (x=0.10, and 0.20) the grain are becomes spheroidal and small as compared to pure $BiFeO_3$ as shows in the fig.4.6(ii) and fig4.6(iii). The grain size of the $Bi_{0.8}Gd_{0.2}FeO_3$ is reduced to 0.50 μm. The finer grain size of the doped samples is the reason for large coercivity in the doped samples.

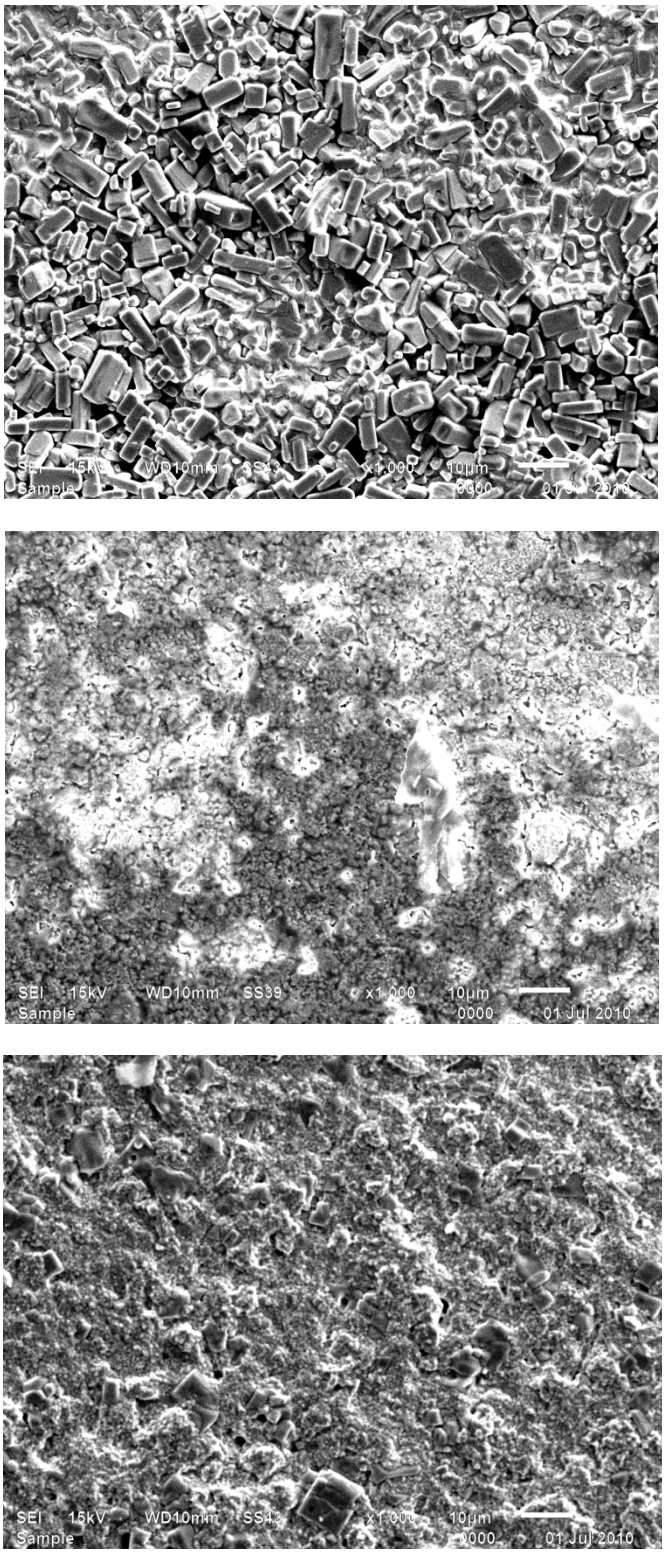

Figure4.6 (i): SEM of samlpes $Bi_{1-}xGdxFeO3$ (*x*=0.0, 0.10, 0.20) at 1000X

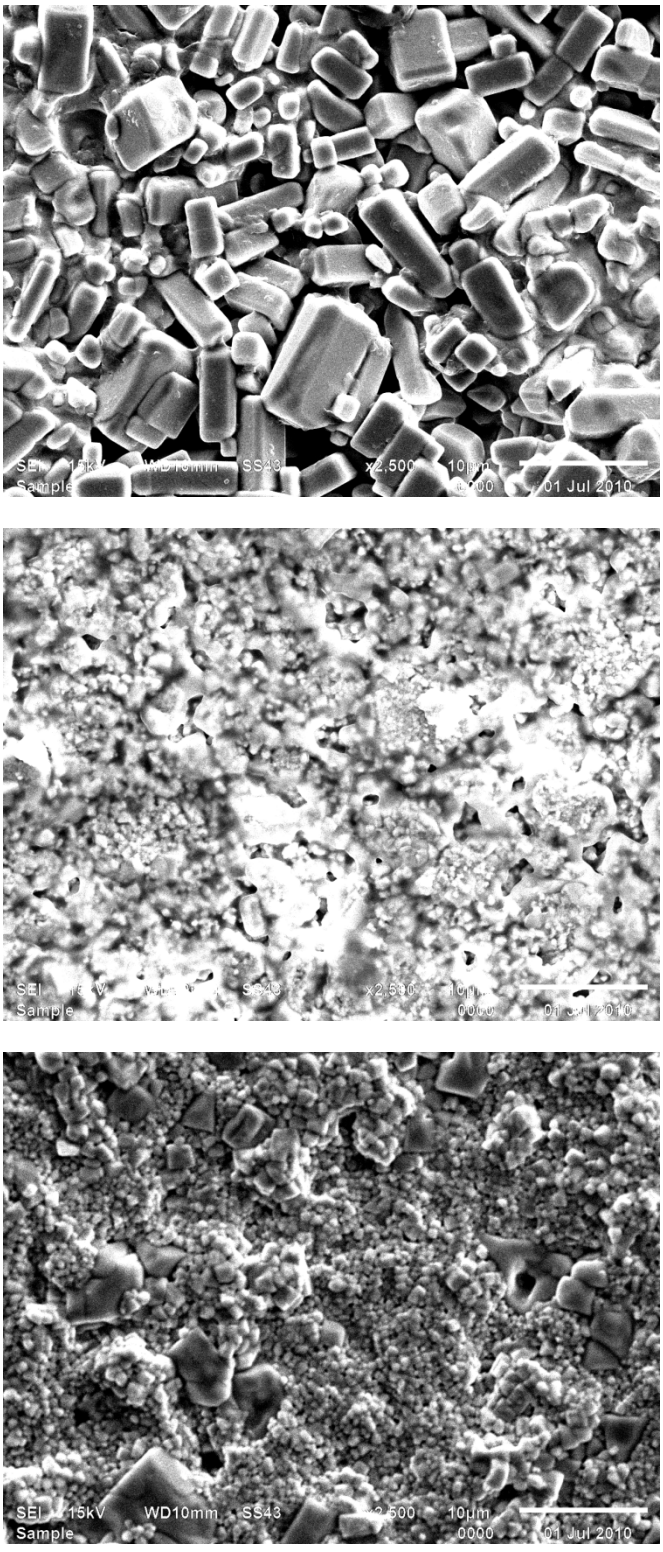

Figure4.6 (ii): SEM of samlpes $Bi_{1-}xGdxFeO3$ (*x*=0.0, 0.10, 0.20) at 2500X

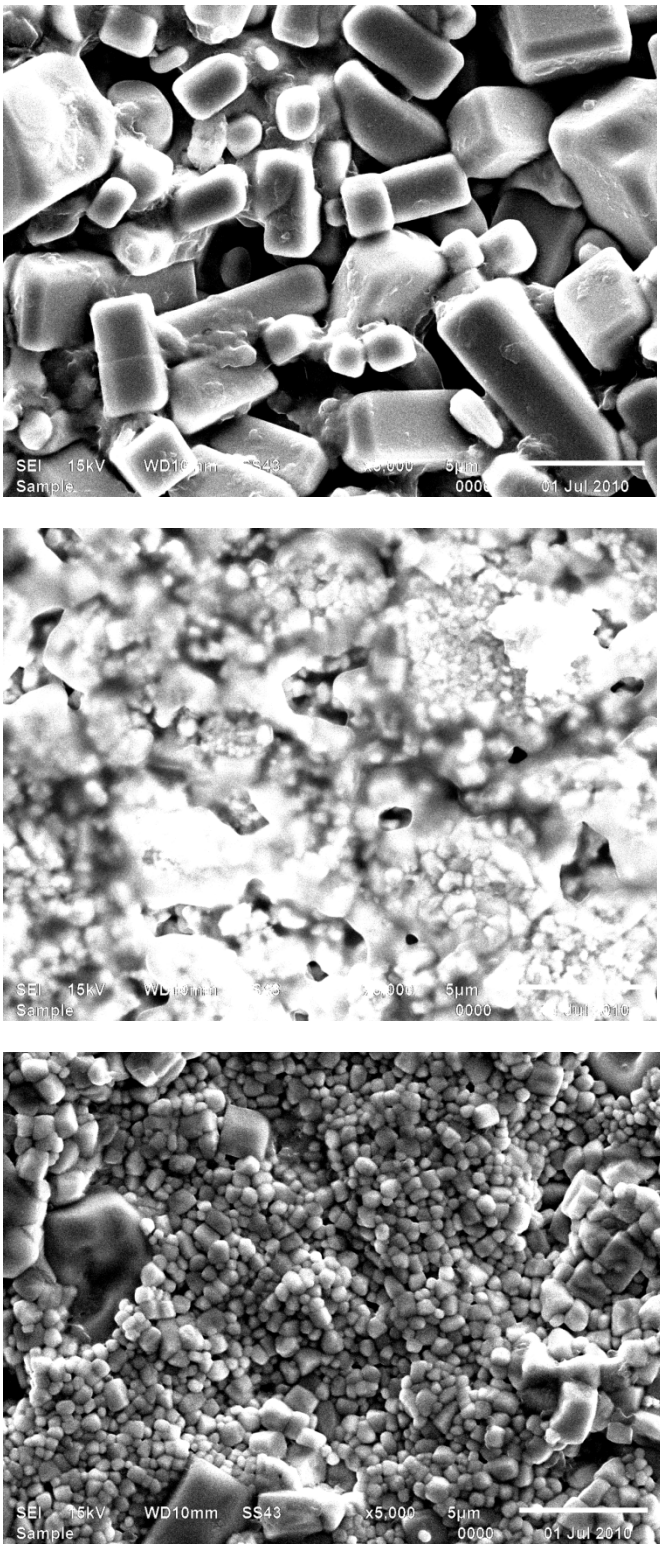

Figure4.6 (iii): SEM of samlpes $Bi_{1-}xGdxFeO3$ (*x*=0.0, 0.10, 0.20) at 5000X

CHAPTER 5

CONCLUSION AND FUTURE WORK

5.1. Conclusion

Multiferroic materials $BiFeO_3$ synthesis by the high energy ball milling (HEBM) and then Gd is doped in A (Bi) site with increasing percent of its molecular weight up to x = 0.05 to 0.20 in $BiFeO_3$. X-ray diffraction is carried out to recognize the crystal structure and present impurity phase. It is seemed that as we doped Gd in $BiFeO_3$ the impurity phase is decrease and we get single phase up to Gd (x = 0.10) and then increase the impurity phase as we increase Gd from x = 0.10 to 0.15, 0.20. The dielectric properties were measured at room temperature of pure $BiFeO_3$ and $Bi_{1-x}Gd_xFeO_3$ in the frequency range from 20Hz to 1MHz. For studied all the samples it is seemed to be as we increase the doping of Gd the dielectric constant increase up to 250 and decrease with respect to frequency and the dielectric losses decrease near about zero with increasing percent of doping. The dielectric constant of pure $BiFeO_3$ is approximately 110 and the dielectric constant of $Bi_{0.9}Gd_{0.1}FeO_3$ is 250 approximately. The dielectric loss of pure $BiFeO_3$ is maximum as compare to $Bi_{1-x}Gd_xO_3$ x = (0.05 to 0.20) in pure $BiFeO_3$ the loss is 0.30 and decrease with respect to frequency range 20Hz to 1MHz, in the other hand $BiFeO_3$ the losses are constant approximately zero with respect to frequency range 20Hz to 1MHz . Therefore the dielectric constant and dielectric losses are strongly dependent upon the concentration of Gd. The P-E loops are also shows that the maximum polarization in $Bi_{0.9}Gd_{0.1}FeO_3$ as we increase the percent of Gd in Bi site the polarization becomes decrease. Scanning electron micrograph of the sample $Bi_{1-x}GdxFeO_3$ (x=0.0, 0.10, 0.20) shows that as we increase the concentration of Gd the shape of the grain becomes rectangular to spherical.

5.2. Future Work

It is seen from the results that rare earth substitution play an important role it tailoring its properties. In this work room temperature measurements were carried out. Therefore high temperature dielectric and magnetic measurements and the effect of sintering temperature on the properties will be the future work. The nanomagnetism properties of the mechanosynthesized multiferroic material with rare earth substitution will be also study in the future.

REFERENCES

1. L. D. Landau and E. M. Lifshitz, Electrodynamics of continuous media (Fizmatgiz, Moscow, 1959) [Amazon][World Cat].

2. I. E. Dzyaloshinskii, Sov. Phys. JETP 10, 628 (1959).

3. H. Schmid, Ferroelectrics, 162, 317 (1994).

4. E. Asher, H. Rieder, H. Schmid, and H. Stossel, Journal of Applied Physics 37, 1404 (1966).

5. G. A. Smolenskii and I. E. Chupis, Sov. Phys. Usp. 25, 475 (1982).

6. J. Wang et al., Science 299, 1719 (2003).

7. T. Kimura et al., Nature 426, 55 (2003).

8. N. Hur et al., Nature 429, 392 (2004).

9. P. Curie, J. Phys. 3, 393 (1894).

10. G. Smolenskii and I. Chupis, Sov. Phys. Uspekhi 25, 475 (1982). Y. Venevtsev and V. Gagulin, Ferroelectrics 162, 23 (1994).

11. M. Fiebig, J. Phys. D 38, R123 (2005). W. Eerenstein, N. D. Mathur, and J. F. Scott, Nature 442, 759765 (2006).

12. R. Smith et al., Journal of Applied Physics 39, 70 (1968).

13. E. Ascher et al., Journal of Applied Physics 37(3), 1404-1405 (1966).

14. G. Smolenskii et al., Soviet Physics-Solid State 1(1), 150-151 (1959).

15. Wang et al., Science 299(5613), 1719-1722 (2003).

16. Hur et al., Nature 429, 392-395 (2004).

17. N. A. Spaldin and M. Fiebig, Science 309, 391 (2005).

18. Hill, N. A. J. Phys. Chem. B 104, 6694–6709 (2000).

19. Hans Schmid, Ferroelectrics 162, 317 (1994).

20. http://www.nanowerk.com/news/newsid=6884.php.

21. In the journal Science ("Low -Magnetic-Field Control of Electric Polarization Vector in a Helimagnet").

22. www.wikkipidia.com.

23. R. Ramesh and N. A Spaldin, Nature Mater. 6, 21 (2007); Ref. (17), No. 434220.

24. Special issue, J. Phys. Condens. Matter 20, 434201–434220 (2008).

25. N. Ikeda et al., J. Phys. Soc. Japan. 69, 1526 (2000); Nature 436, 1136 (2005); Ref. [17], No. 434218.

26. T. Mitsui et al., Ferroelectrics and Related Substances, Landolt-Börnstein, Numerical data and Functional Relations in Science and Technology, New Series Vol. 16 (1) (Springer, Berlin, 1981)[Amazon][WorldCat].

27. N. A. Hill, J. Phys. Chem. B 104, 6694 (2000).

28. N. A. Spaldin, J. Phys. Chem. B 104 (29), 6694-6709 (2000).

29. R. Seshadri, N. A. Hill, Chem. Mater. 13, 2892–2899 (2001).

30. D. V. Efremov, J. van den Brink, and D. I. Khomskii, Nature Mater. 3, 853 (2004).

31. N. Ikeda et al., Nature 436, 1136 (2005).

32. Y. J. Choi et al., Phys. Rev. Lett. 100, 047601 (2008).

33. Hua Wu et al., Phys. Rev. Lett. 102, 026404 (2009).

34. I. A. Sergienko, C. Sen, and E. Dagotto, Phys. Rev. Lett. 97, 227204 (2006).

35. C. W. Nan et al., Journal of Applied Physics 103, 031101 (2008)

36. M. Gajek et al., Nature Materials 6, 296-302 (2007)

37. C. Binek et al., J. Phys. Cond. Mat. 17, L39-L44 (2005)

38. V. L. Mathe, K. K. Patankar, M. B. Kothalei, S. B. Kulkarni, P. B. Joshi and S. A. Patil Indian Academy of Sciences journal Vol. 58 physics pp. 1105–1113.

39. V. R. Palkar, Darshan C. Kundaliya, S. K. Malik, and S. Bhattacharya1 physical review B 69, 212102 (2004).

40. A. K. Pradhan, Kai Zhang, D. Hunter, J. B. Dadson, and G. B. Loutts Journal of Applied Physics 97, 093903 (2005).

41. Jong Kuk Kim, Sang Su Kim, Won-Jeong Kim, Materials Letters 59 (2005) 4006 – 4009.

42. D. H. Wang, W. C. Goh, M. Ning, and C. K. Ong applied physics letters 88, 212907 (2006).

43. Chang Fanggao, Song Guili, Fang Kun, Qin Ping, Zeng Qijun journal of rare earths Vot.24.

44. Shan-Tao Zhang, Yi Zhang, Ming-Hui Lu, Chao-Ling Du, Yan-Feng Chen, Zhi-Guo Liu, Yong-Yuan Zhu, and Nai-Ben Ming applied physics letters 88, 162901 (2006).

45. G. L. Yuan and Siu Wing Ora applied physics letters 89, 052905 (2006).

46. G. L. Yuan and Siu Wing Ora applied physics letters 88, 062905 (2006).

47. G. L. Yuan and Siu Wing Ora applied physics letters 100, 024109 (2006).

48. Deepti Kothari, V. Raghavendra Reddy, Ajay Gupta, Vasant Sathe, and A. Banerjee applied physics letters 91, 202505 (2007).

49. V. A. Khomchenko, D. A. Kiselev, J. M. Vieira, and A. L. Kholkin applied physics letters 90, 242901 (2007).

50. S. R. Das, R. N. P. Choudhary, P. Bhattacharya, and R. S. Katiyar applied physics letters 101, 034104 (2007).

51. W. N. Su, D. H. Wang,a_ Q. Q. Cao, Z. D. Han, J. Yin, J. R. Zhang, and Y. W. Du applied physics letters 91, 092905 (2007).

52. Z. Yan, K. F. Wang, J. F. Qu, and Y. Wanga applied physics letters 91, 082906 (2007).

53. M. Thrall, R. Freer, C. Martin, F. Azougha, B. Patterson, R.J. Cernik, Journal of the European Ceramic Society 28 (2008) 2567–2572.

54. V. A. Khomchenko, D. A. Kiselev, I. K. Bdikin, V. V. Shvartsman, P. Borisov, W. Kleemann, J. M. Vieira, and A. L. Kholkin applied physics letters 93, 262905 (2008).

55. R.K. Mishra, Dillip K. Pradhan, R.N.P. Choudhary, A. Banerjee Journal of Magnetism and Magnetic Materials 320 (2008) 2602– 2607.

56. V. Raghavendra Reddy, Deepti Kothari, Ajay Gupta, and S. M. Gupta applied physics letters 94, 082505 (2009).

57. V.A. Khomchenko, V.V. Shvartsman, P. Borisov, W. Kleemann, D.A. Kiselev, I.K. Bdikin, J.M. Vieira, A.L. Kholkin Acta Materialia 57 (2009) 5137–5145.

58. A.Z. Simoesa, Filiberto Gonzalez Garcia, Carla dos Santos Riccardi, Materials Chemistry and Physics 116 (2009) 305–309.

59. Mansour Al-Haj Cryst. Res. Technol. 45, No. 1, 89 – 93 (2010) / DOI 10.1002/crat.200900550.

60. Yi Dua, Zhen Xiang Chenga, Mahboobeh Shahbazia, Edward W. Collingsb, Shi Xue Doua, Xiao Lin Wanga, Journal of Alloys and Compounds 490 (2010) 637–641.

61. Xiaolong Yan, Jianguo Chen, Yufa Qi, Jinrong Cheng, Zhongyan Meng Journal of the European Ceramic Society 30 (2010) 265–269.

62. V.A. Khomchenko, J.A. Paixa'o, V.V. Shvartsman, P. Borisov, W. Kleemann, D.V. Karpinskyc and A.L. Kholkinc Scripta Materialia 62 (2010) 238–241.

63. Deepam Maurya, Harikrishan Thota, Kanwar Singh Nalwa, Ashish Garg Journal of alloy and compound 477(2009) 780-784.

64. z.K. Cheng, A.H.Li, X.L.Wang, S.K.Dou, K.Ozawa, H. Kimura, S.J. Zhang, and T.R. Shrout Journal of Applied Physics 103, 07E507 (2008)

65. S. kazhugasalamoorthy, S.Dhanuskodi Journal of alloys and compounds 2009